

Most frequently asked questions about the coercivity of Nd-Fe-B permanent magnets

Jiangnan Li , Hossein Sepehri-Amin , Taisuke Sasaki , Tadakatsu Ohkubo  and Kazuhiro Hono 

Elements Strategy Initiative Center for Magnetic Materials (ESICMM), National Institute for Materials Science, Tsukuba, Japan

ABSTRACT

Physically, the coercivity of permanent magnets should scale with the anisotropy field of ferromagnetic compounds, H_A ; however, the typical coercivity values of commercial polycrystalline sintered magnets are only $\sim 0.2 H_A$, which is known as Brown's paradox. Recent advances in multi-scale microstructure characterizations using focused ion beam scanning electron microscope (FIB/SEM), aberration corrected scanning transmission electron microscopy (C_s-corrected STEM), and atom probe tomography (APT) revealed detailed microstructural features of commercial and experimental Nd-Fe-B magnets. These investigations suggest the magnetism of a thin layer formed along grain boundaries (intergranular phase) is a critical factor that influences the coercivity of polycrystalline magnets. To determine the magnetism of the thin intergranular phase, soft X-ray magnetic circular dichroism and electron holography play critical roles. Large-scale micromagnetic simulations using the models that are close to real microstructure incorporating the recent microstructure characterization results gave insights on how the coercivity and its thermal stability is influenced by the microstructures. Based on these new findings, coercivity of Nd-Fe-B magnets is being improved to its limit. This review replies to the most frequently asked questions about the coercivity of Nd-Fe-B permanent magnets based on our recent studies.

ARTICLE HISTORY

Received 18 January 2021
Revised 22 March 2021
Accepted 07 April 2021

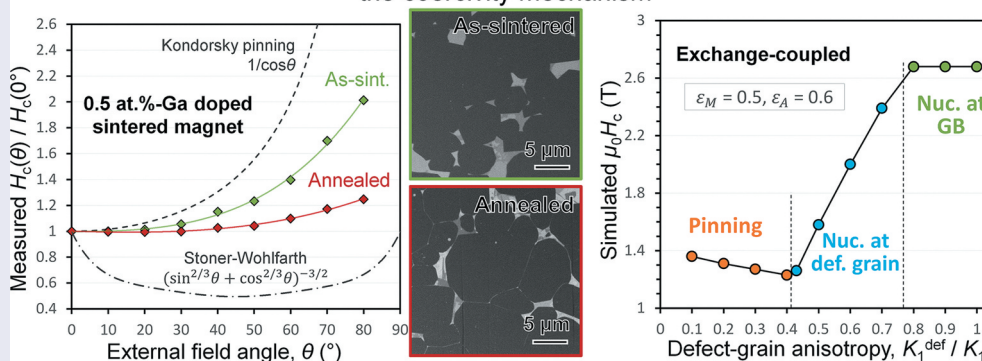
KEYWORDS

Nd-Fe-B magnets; coercivity; thermal stability; microstructure; micromagnetic simulations

CLASSIFICATIONS

50 Energy Materials; Permanent magnets; 203 Magnetics / Spintronics / Superconductors

Development of high coercivity Nd-Fe-B based permanent magnets by controlling the coercivity mechanism



1. Introduction

Nd-Fe-B-based permanent magnets, independently invented by Sagawa [1] and Croat [2] in 1982, are one of the most important industrial materials that are used as magnetic field sources for motor, generator and actuators. It is foreseen that the needs for the high-performance Nd-Fe-B-based permanent magnets will increase further due to the rapid expansion of applications in green energy sectors such as motors and generators for electric vehicles, drones, robots, and wind turbines [3]. Although the maximum energy product of Nd-Fe-B is approaching its theoretical limit, the coercivity that is the most important extrinsic properties for permanent magnet application is still

far below their theoretical limits. Physically, the coercivity of permanent magnets should scale with the anisotropy field of ferromagnetic compounds, H_A ; however, the typical coercivity values of commercial polycrystalline sintered magnets are only around $0.2 H_A$, which is known as Brown's paradox. For example, the typical value of coercivity, $\mu_0 H_c$, for N50 type magnet with $(BH)_{\max} \sim 400 \text{ kJ/m}^3$ is $\sim 1.2 \text{ T}$, which is only $\sim 15\%$ of the anisotropy field of the $\text{Nd}_2\text{Fe}_{14}\text{B}$ compound ($\mu_0 H_A \sim 7.5 \text{ T}$) [4,5]. Due to the thermal demagnetization effect, coercivity decreases to $\sim 0.2 \text{ T}$ at $\sim 160^\circ\text{C}$, which is the operating temperature of the magnet in the traction motor of (hybrid) electric vehicles. The industrial solution for this was to

CONTACT Hossein Sepehri-Amin  h.sepehriamin@nims.go.jp  Elements Strategy Initiative Center for Magnetic Materials (ESICMM), National Institute for Materials Science, Tsukuba 305-0047, Japan

© 2021 The Author(s). Published by National Institute for Materials Science in partnership with Taylor & Francis Group.

This is an Open Access article distributed under the terms of the Creative Commons Attribution License (<http://creativecommons.org/licenses/by/4.0/>), which permits unrestricted use, distribution, and reproduction in any medium, provided the original work is properly cited.

substitute part of Nd in the $\text{Nd}_2\text{Fe}_{14}\text{B}$ lattice with Dy to increase the anisotropy field [4]. The resultant coercivity of $(\text{Nd}_{0.7}\text{Dy}_{0.3})\text{-Fe-B}$ magnets reaches 3.0 T. However, limited natural resources for Dy and its supply risks have raised research interest to develop high coercivity Dy-free Nd-Fe-B magnets with a better thermal stability of coercivity [6,7].

Coercivity is an extrinsic magnetic property and is strongly controlled by microstructure. Intensive researches have been carried out to pursue better understanding of the microstructure–coercivity relationships of Nd-Fe-B magnets. However, due to the limitations of the structural characterization techniques in 1980s, several questions remained unanswered until recently. In this paper, we review recent microstructure investigations and micromagnetic simulations and address answers to the most frequently asked questions about the coercivity of the Nd-Fe-B-based magnets. We will also address how to develop an optimum microstructure that leads to high coercivity without or with minimal use of heavy rare earth (HRE) elements.

2. Why is H_c of sintered magnets only $0.2H_A$?

Nd-Fe-B sintered magnets are produced by a liquid sintering process. Magnetically aligned single crystalline fine particles are isostatically pressured to make a green compact followed by liquid sintering at an elevated temperature of $\sim 950\text{--}1100^\circ\text{C}$. The Nd-Fe-B magnets right after the sintering process show a very small coercivity of $\sim 0.8\text{--}0.9$ T. After annealing the as-sintered magnets at $\sim 520\text{--}600^\circ\text{C}$, coercivity increases by $\sim 25\text{--}30\%$ [8–20]. Typical microstructure of Nd-Fe-B sintered magnets, shown in Figure 1 is comprised of $\text{Nd}_2\text{Fe}_{14}\text{B}$ grains separated with thin intergranular phase. In addition, secondary Nd-rich phase grains including metallic Nd, NdO_x , and NdFe_4B_4 exist in the microstructure. BSE-SEM observations by Vial

et al. convincingly showed the coercivity increase upon post-sinter annealing was attributed to the formation of a continuous intergranular phase to isolate $\text{Nd}_2\text{Fe}_{14}\text{B}$ grains [12]. This intergranular phase was assumed to be Nd-rich based on the contrast in the BSE-SEM images. The structure of the intergranular phase was identified to be amorphous by Li et al. using high-resolution TEM as shown in Figure 2(a,c) for the as-sintered and optimally post-sinter annealed samples [19]. The mechanism of the formation of the intergranular phase was elaborated by Sepehri-Amin et al. to be the Nd/NdCu eutectic reaction; using three-dimensional atom probe (3DAP), they found NdCu precipitates coexist with metallic Nd at the triple junctions of the as-sintered magnet, which melt at the temperatures above 520°C during post-sinter annealing and infiltrate into the grain boundaries to form thin intergranular phase [21].

Although the presence of the intergranular phase was known from the early study of Nd-Fe-B sintered magnets [12,22], its chemical composition and the magnetism have not been determined until recently. The 3DAP study by Sepehri-Amin et al. showed the grain boundaries in as-sintered magnet has only slight segregation of Nd without forming any distinct phase. However, a distinct amorphous phase was observed along the grain boundaries in the post-sinter annealed samples with an average thickness of ~ 3 nm. This phase was identified to be amorphous containing over 65 at.% of Fe and Co as shown in Figure 2(b,d) [21]. In order to estimate the magnetization of the intergranular phase, a thin film with the identical chemical composition as the intergranular phase determined by 3DAP, $\text{Nd}_{29.9}\text{Fe}_{65.8}\text{B}_{3.1}\text{Cu}_{1.2}$, was prepared. The amorphous film was found to be ferromagnetic with the magnetization of 0.6 T [21]. This work suggested that the $\text{Nd}_2\text{Fe}_{14}\text{B}$ grains in optimally annealed sintered magnets are exchange coupled through the thin ferromagnetic intergranular phase.

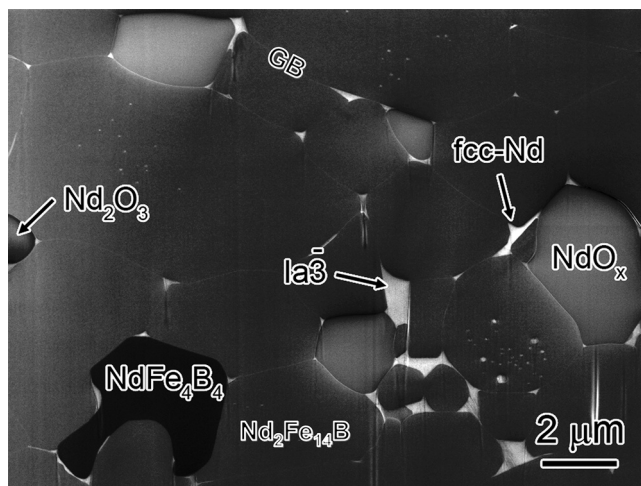


Figure 1. In-lens secondary electron SEM image showing general microstructure of typical Nd-Fe-B sintered magnet. Reproduced by permission from [28], copyright (2016, Elsevier).

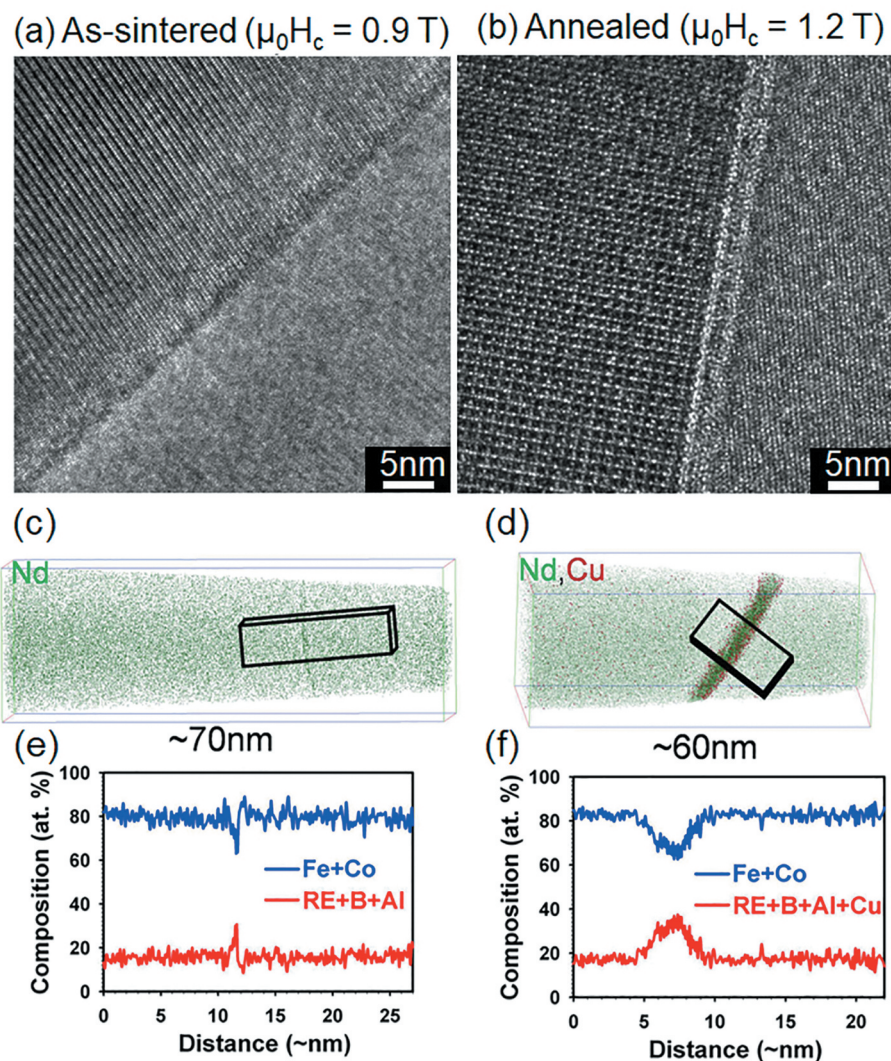


Figure 2. High-resolution TEM, atom probe tomography and composition line profile obtained from intergranular phase of (a, b) as-sintered and (c, d) optimally annealed Nd-Fe-B sintered magnet. Reproduced from Li et al. [19] and Sepehri-Amin et al. [21] with copyright permissions from Elsevier.

Motivated by this work, direct measurements of the magnetism of the thin intergranular phase of Nd-Fe-B sintered magnets were carried out using various techniques. Nakamura et al. employed surface-sensitive soft X-ray magnetic circular dichroism (XMCD) to intergranularly fractured surface of Nd-Fe-B sintered magnets and found that the intergranular phase in the sintered magnets have a saturation magnetization of ~ 1.0 T at room temperature with a Curie temperature of $\sim 260^\circ\text{C}$ as shown in Figure 3 [23]. Kohashi et al. [24] and Murakami et al. [25] also reported ferromagnetic nature of the intergranular phase in Nd-Fe-B sintered magnets using spin-polarized scanning electron microscopy and electron holography, respectively. Note that the absolute value of the magnetization of the intergranular phase changes depending on the measurement technique such as XMCD, electron holography, or spin-polarized SEM which can originate from experimental errors in each technique and/or the fluctuation in the composition of the studied intergranular phase. However, all these

measurements agree with each other on the ferromagnetic nature of the intergranular phase in Nd-Fe-B sintered magnets. Based on these studies, the unexpectedly low coercivity of Nd-Fe-B sintered magnets is concluded to be due to the ferromagnetic nature of the intergranular phase which can work as only weak pinning sites against magnetic domain wall (DW) motions during demagnetization process. Micromagnetic simulation results predict that the formation of nonferromagnetic intergranular phase which can exchange-decouple $\text{Nd}_2\text{Fe}_{14}\text{B}$ grains would lead to a substantial increase of the coercivity of the sintered magnets [26,27].

Using high angle annular dark field (HAADF) STEM and STEM-EDS studies, Sasaki et al. showed that the chemical composition of the intergranular phase in Nd-Fe-B sintered magnets varies depending on their angles with respect to the easy axis of the $\text{Nd}_2\text{Fe}_{14}\text{B}$ grains; more enriched with Nd in the grain boundaries located perpendicular to the c-axis of $\text{Nd}_2\text{Fe}_{14}\text{B}$ grains while its Nd content is lower in the

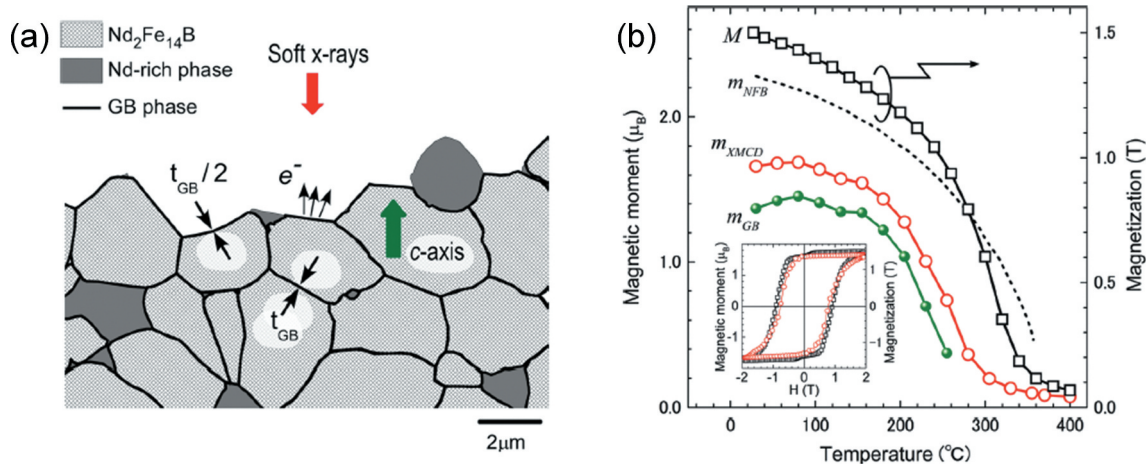


Figure 3. (a) Schematic diagram of XMCD measurement on fractured surface of magnet. (b) Temperature dependence of Fe magnetic moments in the GB phase (m_{GB}) estimated for $t_{\text{GB}} \sim 3$ nm. m_{XMCD} is the Fe magnetic moment, m_{NFB} corresponds to the magnetic moment averaged over Fe sites in $\text{Nd}_2\text{Fe}_{14}\text{B}$ crystal. The inset represents the magnetic field dependences of m_{XMCD} (open circles) and M (open squares) recorded at 30°C. Reproduced by permission from [23], copyright (2014, AIP Publishing).

intergranular phase formed parallel to the *c*-axis of the grains (Figure 4) [28]. Such variations of the composition of the intergranular phase are expected to influence its magnetization. Based on thin film experiments, Sakuma et al. showed that the amorphous $\text{Fe}_{1-x}\text{Nd}_x$ phase is ferromagnetic for $x < 0.7$ in agreement with first-principles calculation results, indicating Nd concentration higher than 70% is required to decouple the intergranular exchange (Figure 5) [29].

The addition of a small amount of Ga to Nd-Fe-B sintered magnets has been known to increase the coercivity by improving the wettability of the

intergranular phase during post-sinter annealing [30–33]. In earlier development of Nd-Fe-B sintered magnets, priority has been given to the achievement of high remanence. Then, part of Nd was replaced with Dy for increasing the coercivity. As a result, the chemical composition of the N50 type sintered magnet was around $\text{Nd}_{13.9}\text{Fe}_{79.5}\text{B}_6\text{Cu}_{0.1}$, which is slightly richer in Nd with respect to the stoichiometry of $\text{Nd}_2\text{Fe}_{14}\text{B}$, $\text{Nd}_{11.7}\text{Fe}_{82.4}\text{B}_{5.8}$. In order to increase the coercivity of the Nd-Fe-B sintered magnet without using Dy, Nakajima et al. developed a Nd-rich and B-lean alloy with a trace Ga addition, i.e. $\text{Fe}_{77.6}\text{RE}_{14.8}\text{B}_{5.1}\text{Cu}_{0.1}\text{Ga}_{0.5}$ as strip cast alloy for Nd-Fe-B sintered magnet

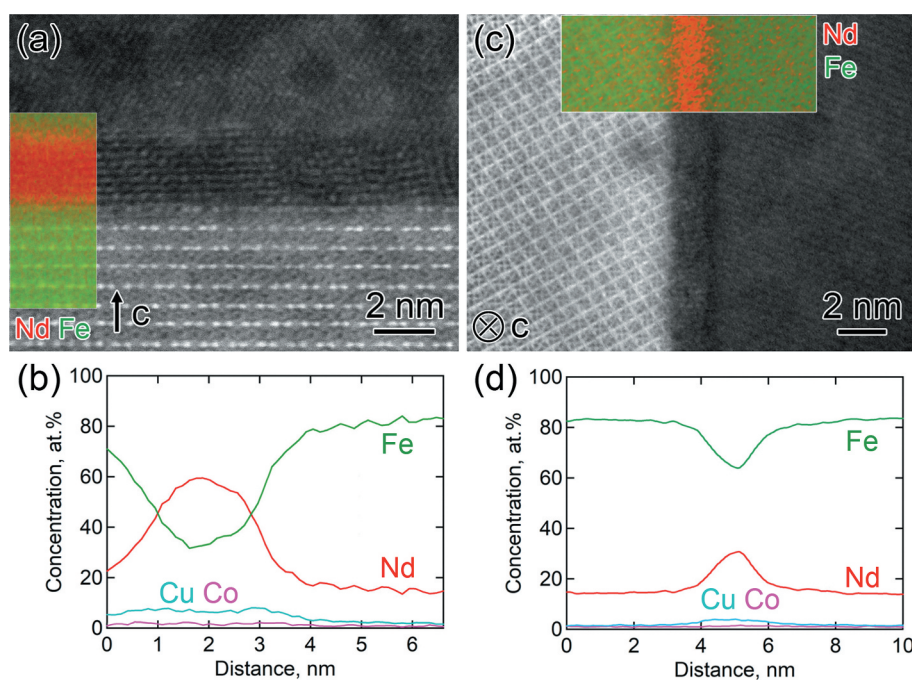


Figure 4. HAADF-STEM images, super imposed STEM-EDS maps, and composition line profiles obtained from EDS maps showing intergranular phase in Nd-Fe-B sintered magnets located (a, b) at the *c*-plane and (c, d) at the side plane of $\text{Nd}_2\text{Fe}_{14}\text{B}$ grains. *c*-axis in $\text{Nd}_2\text{Fe}_{14}\text{B}$ grain is shown with a white arrow. Reproduced by permission from [28], copyright (2016, Elsevier).

with a substantially improved coercivity of 1.8 T for the grain size as large as $\sim 5 \mu\text{m}$ [34]. Microstructure investigations by Sasaki et al. (Figure 6) showed the formation of three types of nonferromagnetic intergranular phases ($\text{Ia}\bar{3}$, amorphous Nd-rich, and $\text{Nd}_6\text{Fe}_{13}\text{Ga}$ phases) are the main reason for the substantial enhancement of coercivity to 1.8 T upon post-sinter annealing [35]. Niitsu et al. also [36] also reported these three types of the intergranular phases are non-ferromagnetic using electron holography. Magneto-optical Kerr effect microscopy by Soderznic et al. showed that the formation of thick non-ferromagnetic intergranular phase suppressed the cascade propagation of magnetic domains during the demagnetization process, which was considered to be responsible for the enhancement of coercivity [37].

In short, low coercivity, $0.2 H_A$, of the Nd-Fe-B sintered magnet with respect to the anisotropy field of the $\text{Nd}_2\text{Fe}_{14}\text{B}$ phase is due to the intergranular exchange coupling through ferromagnetic intergranular phase.

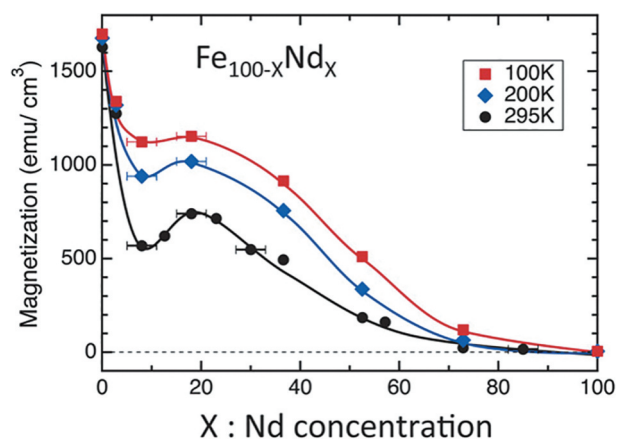


Figure 5. Saturation magnetization of $\text{Fe}_{100-x}\text{Nd}_x$ films as a function of Nd content at the temperatures of 100, 200, and 295 K. Reproduced by permission from [29], copyright (2016, IOP Publishing).

3. Why does grain size reduction lead to increase in H_c ?

It is well known that the coercivity of anisotropic Nd-Fe-B-based magnets increases as grain size reduces as shown in Figure 7 [35,38–40]. The reason for this linear coercivity increase upon reduction of grain size, expressed as $H_c = a - b \ln D$ by Ramesh et al. [38], was explained due to the reduction of defect densities in exchange decoupled $\text{Nd}_2\text{Fe}_{14}\text{B}$ grains. However, as described above, the recent investigations showed that the $\text{Nd}_2\text{Fe}_{14}\text{B}$ grains are exchange coupled in anisotropic Nd-Fe-B sintered magnets and the reduction of defect densities cannot explain the grain size dependence of coercivity. Moreover, coercivity decrease was reported for the grain size below $3 \mu\text{m}$ deviating from the linear grain size dependence of coercivity (Figure 7). Li et al. reported the reduction of the coercivity in the fine grain-sized Nd-Fe-B sintered magnets produced by conventional powder processing routes is due to the oxidation of metallic Nd during the sintering process resulting in the lack of Nd-rich intergranular phase [41]. As discussed in the previous section, metallic Nd coexisting with NdCu is necessary for the uniform formation of the intergranular phase. When metallic Nd is oxidized, the eutectic melting of Nd/NdCu does not occur during the post-sinter annealing process. In order to suppress the reduction of coercivity in $D < 3 \mu\text{m}$, the oxidation of the metallic Nd phase during the powder metallurgy process must be suppressed. To overcome this problem, Une et al. prepared ultrafine grained ($D < 1 \mu\text{m}$) $\text{Nd}_2\text{Fe}_{14}\text{B}/\text{Nd}$ powders by He-jet milling and sintered the powders using the press-less sintering process in Ar atmosphere [42]. This led to the realization of ultrafine grained sintered magnets with $D \sim 1 \mu\text{m}$, and the coercivity of 2 T was demonstrated without alloying any HRE elements. A similar trend of grain size dependence of coercivity was also reported in the Ga-doped Nd-rich B-lean Nd-Fe-B sintered magnets in which a better magnetic isolation of Nd_2

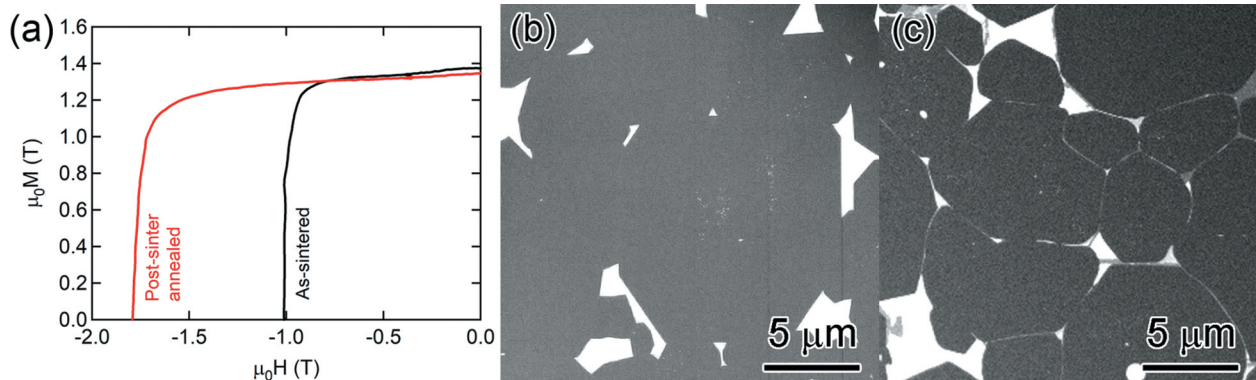


Figure 6. (a) Demagnetization curves for as-sintered and post-sinter annealed Ga-doped Nd-rich Ga-lean Nd-Fe-B sintered magnets. Backscattered electron SEM images taken from (b) as-sintered and (c) post-sinter annealed samples. Reproduced by permission from [35], copyright (2016, Elsevier).

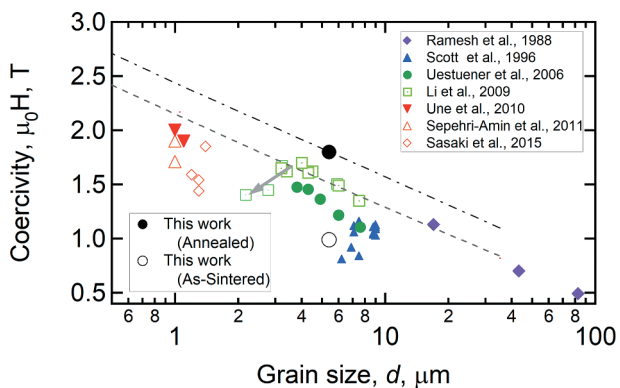


Figure 7. Grain size dependency of coercivity of exchange-coupled and exchange-decoupled Nd-Fe-B sintered magnets. Reproduced by permission from [35], copyright (2016, Elsevier).

Fe_{14}B grains is realized via the formation of $\text{Nd}_6\text{Fe}_{13}\text{Ga}$ intergranular phase as shown in Figure 7 [35]. However, the underlying physics for this grain size dependence of coercivity had not been explicitly explained. Based on the 2D micromagnetic simulations, Schrefl et al. showed a long-range magnetic interaction exists among $\text{Nd}_2\text{Fe}_{14}\text{B}$ grains which becomes less effective as grain size decreases; as a result, the demagnetization field decreases in the smaller grain-sized magnets [43]. Sepehri-Amin et al. employed 3D micromagnetic simulations and qualitatively reproduced the grain size dependence of coercivity in the exchange-coupled anisotropic Nd-Fe-B sintered magnets [44]. Coercivity is often expressed as $H_c(T) = \alpha H_A(T) - N_{\text{eff}} M_s(T)$ in which the first term is the influence of the defects and grain misalignment on the anisotropy field and the second term is related to the reduction of coercivity due to the demagnetization field [45]. Micromagnetic simulations on the exchange-coupled Nd-Fe-B sintered magnets have shown that improved coercivity by the reduction of the grain size is due to the lower effective demagnetization constant, N_{eff} , as shown in Figure 8. This means that the effective demagnetization field, $N_{\text{eff}} M_s$, decreases as the grain size decreases, giving rise to a larger coercivity for smaller grain size. In the Nd-Fe-B sintered magnets, due to the surface machining or oxidations, the surface grains have reduced anisotropy field and hence almost no coercivity. Hence, the surface grains become multidomain at a remanent state and their magnetization reversal occurs at a much lower magnetic field than the nucleation field during the demagnetization process as often observed in the magneto optical Kerr effect microscopy (shown in Figure 9(a)). XMCD measurement by Billington et al. [46] also showed the multidomain grains with small coercivity on the polished surface. Nevertheless, the surface coercivity of the fractured surface on which Nd-rich intergranular phase still exist show comparable coercivity to that of bulk value [46]. The reversed

grains on polished surface cause stray field to the surrounding grains. Sepehri-Amin et al. calculated the stray field generated by the reversed surface grain [44]. The distribution of the demagnetization vectors shown in Figure 9(b) and calculated distribution of the stray field at the surrounding of the reversed grains is shown in Figure 9(c). These simulations showed that the coercivity increase with decreasing grain size is due to the reduction in the effective stray field arising from the neighboring grains. Upon reduction of the grain size, the maximum stray field which is at the interface with the reversed neighboring grains decreases. Larger stray field produced by the larger sized grains assist the magnetization reversal of the neighboring grains which is detrimental to coercivity.

In short, early and more recent micromagnetic simulations works for polycrystalline anisotropic magnets confirmed the grain size dependence of the coercivity of anisotropic sintered magnets is explained by the reduction of stray field with decreasing grain size.

4. Why does HRE grain boundary diffusion process increase H_c ?

Since the first report by Park et al. [47], grain boundary diffusion (GBD) process using HRE elements has been developed as an HRE-efficient technique to enhance the coercivity of Nd-Fe-B magnet. In this process, Nd-Fe-B sintered magnets are coated with Dy or Tb in the form of oxide, fluoride, or pure metals then undergo a subsequent heat treatment [48–52], i.e. heat-treated at elevated temperature of 800–1000°C for 3–10 h followed by an optimum post-sinter annealing which results in the diffusion (infiltration) of HRE into the magnet and the formation of HRE-enrich shell in $\text{Nd}_2\text{Fe}_{14}\text{B}$ grains [53,54]. The coercivity of the magnet is increased due to the formation of HRE-enriched high- H_A shell; meanwhile, the loss of remanent magnetization due to the antiferromagnetic coupling of Dy with Fe in the 2:14:1 phase is minimized since only a small amount of HRE is locally utilized in the shell of the 2:14:1 grains. Although the GBD process is now widely used to manufacture high-coercivity Nd-Fe-B sintered magnets for traction motor and wind turbine applications, the underlying mechanism for the formation of unique HRE-rich shell structure and the upper limit of coercivity using this method have not been well understood.

In order to understand the effect of coercivity increase in the course of the entire diffusion process including the Dy-diffusion and subsequent heat-treatment process, Kim et al. investigated the coercivity change in each step for Dy-free and Dy-containing samples and their microstructure change in details [55]. Figure 10(a) shows the coercivity as function of the amount of Dy diffusion applied to two types of initial samples: one is Dy-free Nd-Fe-B and the other

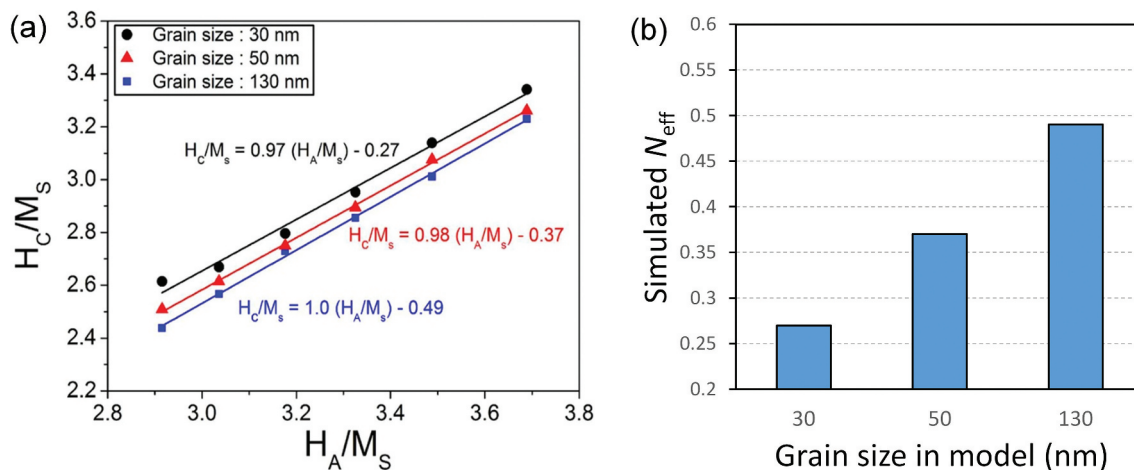


Figure 8. (a) H_c/M_s as a function of H_A/M_s of the micromagnetic models with an average grain size of 30, 50, and 130 nm. The micromagnetic parameters of a and N_{eff} are measured from the slope and intercept of a linear fit to this graph [44]. (b) Simulated N_{eff} at different modeled grain sizes. Reproduced by permission from [44], copyright (2014, Elsevier).

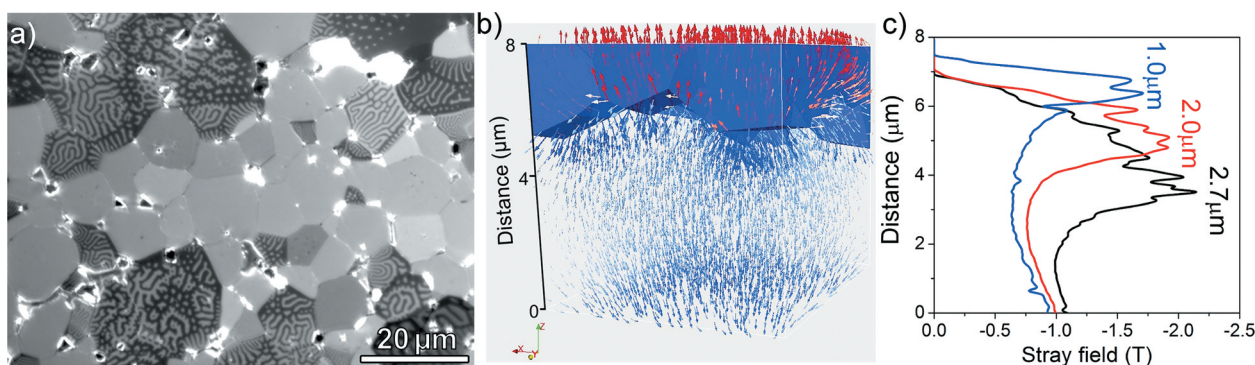


Figure 9. (a) Magneto optical Kerr effect (MOKE) microscopy of the surface of Nd-Fe-B sintered magnet in the remanent state after full magnetization under 5 T magnetic field and (b) simulations of stray field from the surface grain to the interior grains in anisotropic sintered magnet and (c) calculated maximum stray field from cross-sectional slices at $Z = 0$ to $Z = 8 \mu\text{m}$ for different grain sizes. Reproduced by permission from [44], copyright (2014, Elsevier).

is Dy-containing $\text{Nd}_{24.3}\text{Dy}_{7.5}\text{Fe}_{66.0}\text{B}_{1.0}\text{Cu}_{0.1}\text{Al}_{0.15}\text{Co}_{0.9}\text{Ga}_{0.05}$ (wt.%) sintered magnets. Coercivity increases as the amount of Dy supply increases and it eventually reaches saturation. As shown in Figure 10(b), when GBD process is applied to the Dy-free sample, the coercivity does not increase to more than 2.1 T. On the other hand, when 0.1 wt.% Dy is diffused to the Dy-containing sample with the initial coercivity of 2.3 T, the coercivity reaches 3 T. In order to reduce the amount of Dy from the GBD processed high coercivity magnet, it is desirable to increase the coercivity to higher than 3 T without alloying Dy in the starting sample. It is also known that the high coercivity can be achieved only when the sample is optimally heat-treated after the diffusion process [55]. Based on the STEM-EDS elemental analyses as shown in Figure 10 (c,d), they found that post-annealing after Dy-diffusion leads to the formation of a secondary Dy-rich shell, which indicates a solid diffusion of Dy atoms from the GB to the shell region during the annealing process. As a result, the Nd concentration

in the intergranular phase increased substantially compared to the as GBD treated sample because the Nd atoms rejected from the Dy-rich shell are enriched in the intergranular phase, which also leads to the formation of thicker intergranular phase with higher Nd concentration.

One of the long-standing questions on the HRE GBD process was the formation mechanism of a unique shell structure that is asymmetric with respect to grain boundaries. Seelam et al. [56] proposed that the HRE-rich shell is formed by the solidification of liquid phase during cooling from the processing temperature, thereby explaining the sharp core/shell interface and faceted core shape. However, this does not explain the anisotropic nature of the HRE-rich shell around grain boundaries and apparently large fraction of the HRE-rich shell near the surface of GBD processed magnets. Recently, Kim et al. investigated the formation mechanism of Tb-rich shell in a Tb-diffusion processed Nd-Fe-B sintered magnet based on detailed

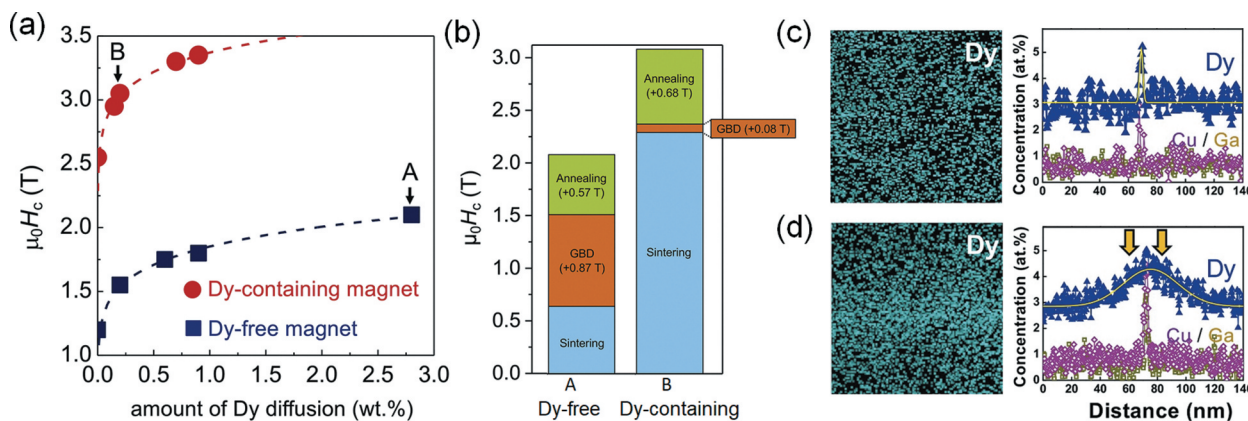


Figure 10. (a) Variations in coercivity as functions of the amount of Dy diffusion for GBD processed Dy-free and Dy-containing magnets. (b) $\Delta\mu_0 H_c$ of samples A and B in (a) with GBD process steps (GBD treatment and post-diffusion annealing). EDS elemental map of Nd and EDS line profiles across GB phase in (c) GBD treated and (d) post-diffusion annealed Dy-free magnet. Reproduced by permission from [55], copyright (2019, Elsevier).

microstructure characterization using STEM and phase-field simulation [57]. As shown in Figure 11, the formation of Tb-rich shell for the former is always asymmetrical along the GB. Inside the shell, the concentration of Tb gradually increases from the GB side to the core/shell interface then abruptly drops in the core range (see Figure 11(c)). Further TEM observation showed the existence of the stacking faults at the core/shell interface [57]. To explain these microstructure features, Kim et al. proposed the chemically induced liquid film migration (CILFM) mechanism to explain the Tb-rich shell formation. As shown in the phase-field simulation (Figure 12(a)), the grain grows by the migration of liquid film GB at the processing temperature. A continuous decrease of Tb concentration from core/shell interface to grain surface is then found in the shell as shown in Figure 12(b) in agreement with the experimental observation.

In short, the coercivity enhancement of HRE GBD processed magnets are not only due to the formation of the HRE-rich shell, but also due to the formation of the Nd-rich intergranular phase by the optimal post-diffusion annealing. The HRE-rich shell is formed by the CILFM, which explains the asymmetric feature of the HRE-rich shell.

5. How to increase the coercivity of hot-deformed magnets using HRE diffusion bypassing grain coarsening?

HRE GBD is expected to increase the H_c of hot-deformed magnet as well. However, the conventional HRE GBD process applied on sintered magnets fail on the hot-deformed magnets as shown in Figure 13(a), where Dy-vapor diffusion gives rise to negligible increases of H_c as the result of the coarsening of grains at the high processing temperature of $\sim 900^\circ\text{C}$. In order to reduce the process temperature to suppress the grain coarsening (see Figure 13(c)) of the hot-deformed magnets, Sepehri-Amin et al. [58] applied a low-temperature eutectic diffusion process. This method is an extension of the Nd-Cu eutectic diffusion process that was invented to enhance the coercivity of HDDR powder [59] as well as hot-deformed magnets [60] without using HRE. High H_c value of 2.3 T or 2.5 T was reported after the diffusion with $\text{Nd}_{70}\text{Cu}_{30}$ [60] or $\text{Nd}_{90}\text{Al}_{10}$ [61] alloys. By adding HRE to the eutectic alloys like $\text{Nd}_{60}\text{Dy}_{20}\text{Cu}_{20}$ [58], $\text{Nd}_{62}\text{Dy}_{20}\text{Al}_{18}$ [62] and $\text{Nd}_{60}\text{Tb}_{20}\text{Cu}_{20}$ [63], the coercivity was further enhance to 2.6–2.8 T at a processing temperature $\leq 700^\circ\text{C}$ accompanied by a loss of remanence. This loss of remanence is more serious compared to the conventional HRE GBD

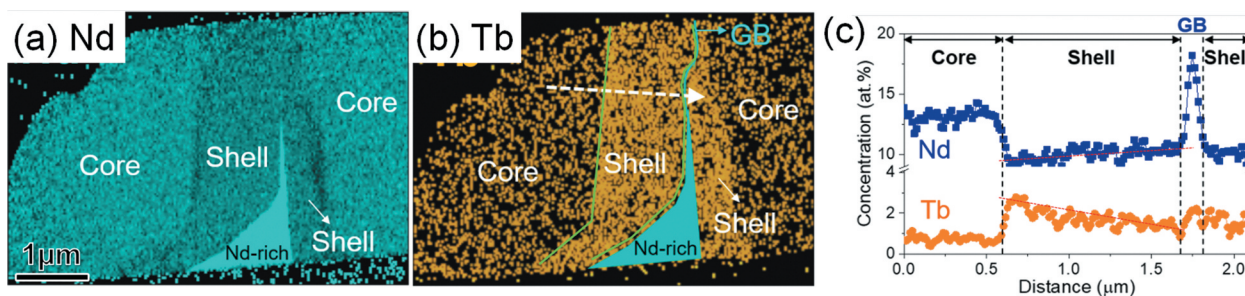


Figure 11. EDS elemental map for (a) Nd and (b) Tb. The line scan profile of Tb across the shell (dashed line in Tb map) is shown in (c). Reproduced by permission from [55], copyright (2019, Elsevier).

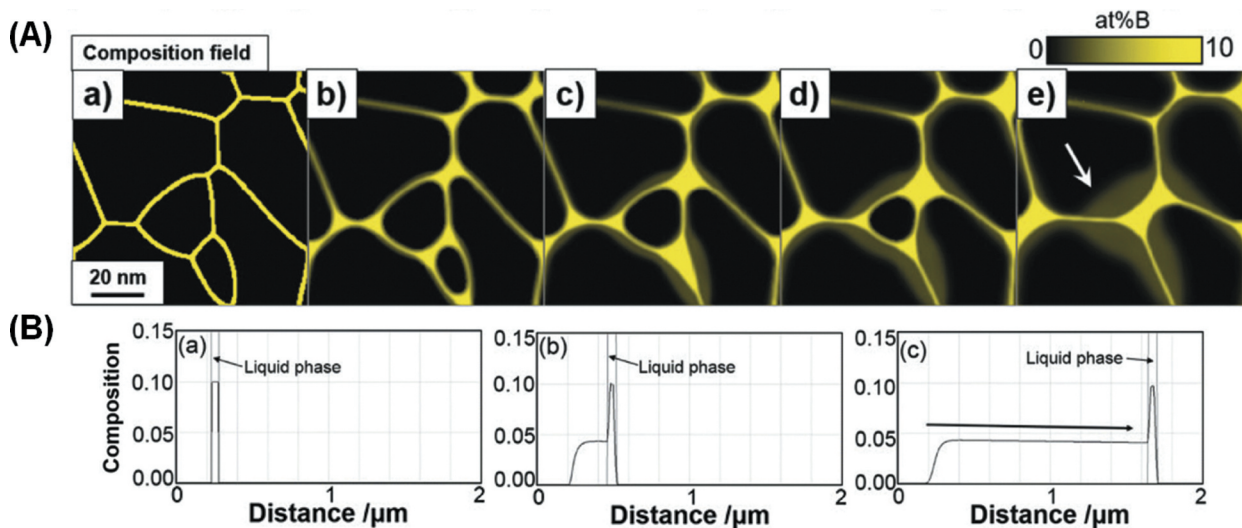


Figure 12. (a) 2D phase-field simulation of the microstructure changes based on the CILFM mechanism during isothermal ageing for (a) $t' = 0$, (b) $t' = 0.5$, (c) $t' = 2.5$, (d) $t' = 5$, and (e) $t' = 10$ (t' is dimensionless time). (b) 1D phase-field simulation of the real scale calculation on the shell formation process during isothermal ageing for (a) $t' = 0$, (b) $t' = 5 \times 10^3$, and (c) $t' = 3 \times 10^4$ (t' is dimensionless time). Reproduced by permission from [57], copyright (2020, Elsevier).

process applied to sintered magnets, which is attributed to the formation of thick Nd-rich nonferromagnetic intergranular phases observed in the eutectic diffusion processed hot-deformed magnets. Although the formation of HRE-rich shell was found, only a few grains are fully enveloped by HRE-enriched shell in Figure 13(b), and most of the platelet-shaped grains are partly covered either on the sides or on the c -plane surfaces [62,63]. Micromagnetic simulations [63] suggested that these high- H_A shell can obstruct the propagation of magnetic DWs if the 2:14:1 grains are exchange coupled, or can force a relocation of nucleation site from grain surface to the core/shell interface if the grains are exchange decoupled.

In short, GB infiltration of low melting temperature Nd-HRE-(Cu,Al) eutectic alloys leads to a substantial increase of coercivity of hot-deformed magnets without inducing grain coarsening.

6. What is the coercivity mechanism of Nd-Fe-B magnets?

The magnetization reversals in permanent magnets should at least consist of two steps: the nucleation of reversed domain and the propagation of DW throughout the matrix. Depending on which step controls the magnetization reversal, the coercivity mechanism is generally described as nucleation-control or DW pinning-control. In early studies of Nd-Fe-B sintered magnets with a large grain size of $\sim 5\text{--}10 \mu\text{m}$, the measured initial magnetization curve from a thermally demagnetized state always shows a large susceptibility, and the magnetization is easily saturated after applying a small external magnetic field. This ‘one-step’ initial magnetization curve was explained as evidence for the lack of effective DW pinning sites, indicating the nucleation-control reversal mechanism [45,64]. However, Hadjipanayis et al.

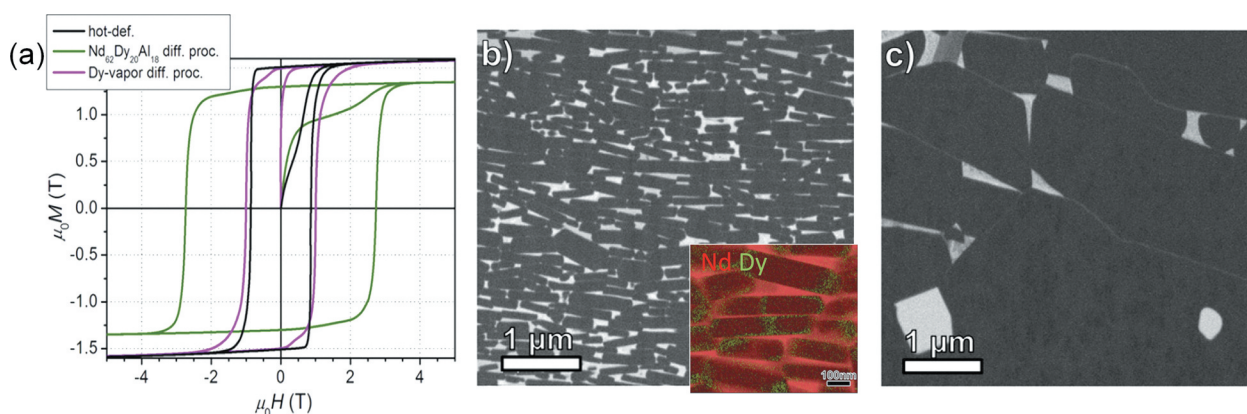


Figure 13. (a) Magnetization curves of hot-deformed, Nd-Dy-Al diffusion-processed and Dy-vapor diffusion-processed magnet samples. (b) BSE-SEM image of $\text{Nd}_{62}\text{Dy}_{20}\text{Al}_{18}$ eutectic diffusion-processed hot-deformed magnet. The inset shows the TEM-EDS elemental mapping image. (c) BSE-SEM image of Dy-vapor diffusion-processed hot-deformed magnet. Reproduced by permission from [62], copyright (2017, Elsevier).

argued that the ‘one-step’ feature only demonstrated the lack of pinning site inside the large-size grains, while pinning of DW along grain boundaries is still possible [65]. Evidence for the latter has been found in the recently developed sintered magnet with an ultra-fine grain size of 1 μm [66] and in the hot-deformed magnet with submicron grain size [67]. These grain sizes are comparable to the domain size of thermally demagnetized Nd₂Fe₁₄B so after initial DW displacements in the matrix, they are pinned at grain boundaries. This gives rise to the ‘two-step’ initial magnetization curves consisting of initial high susceptible region in the low magnetic field, where DWs in multidomain size grains displaces, and the susceptibility become low as the DW are pinned at grain boundaries. When the DWs are de-pinned, magnetization again increases to saturation as shown in Figure 14(a, b). The micromagnetic simulations on the grain size dependence of initial curve by Sepehri-Amin et al. reproduced the two-step initial magnetization curves as shown in Figure 14(c) [44], where ‘one-step’ initial curve transfers to ‘two-step’ shape when grain size reduces smaller than 1 μm. Note that the grain size where the ‘two-step’ feature appears for both experimental curves and simulation curves is apparently larger than the conventionally defined single-domain size, $D_c = \frac{72\sqrt{AK}}{\mu_0 M_s^2} \approx 200\text{nm}$ for Nd₂Fe₁₄B, which is valid to determine the single-domain size of a magnetized particle [68] but improper for the discussion of ‘two-step’ feature here.

Another method to characterize the magnetization reversal mechanism in the ferromagnetic materials is based on angular dependence of coercivity [69–73]. Stoner–Wohlfarth model [74], which describes the coherent reversal with uniaxial anisotropy energy $K_u = K_1 \sin^2\theta$, gives a $H_c(\theta)$ curve with a local minimum at $\theta = 45^\circ$. Another model named after Kondorsky to describe the DW depinning process gives $H_c(\theta) = \frac{E_b}{\cos\theta} \propto \frac{1}{\cos\theta}$ that assumes a fixed energy barrier E_b despite the change of field angle θ . Micromagnetic simulations [75,76] show that the simulated $H_c(\theta)$ of a large size system does not strictly

follow the results of simple model. However, the shape of $H_c(\theta)$ curve still correlates strongly with coercivity mechanism. Bance et al. [75] showed the shift of $H_c(\theta)$ curve from Stoner–Wohlfarth-like to Kondorsky-like by reducing the thickness of soft defect layer in a single Nd₂Fe₁₄B grain model. However, this simulation was carried out on a single crystal model. For simulating the magnetization behaviors of actual permanent magnets, the model must be exchange-coupled anisotropic polycrystals. Li et al. [76] showed a direct correlation between reversal mechanism and the appearance of local minimum in $H_c(\theta)$ based on the simulations of a polycrystalline model (see Figure 15 (b,c)). Experimentally measured $H_c(\theta)$ of both conventional sintered and hot-deformed magnets are found to monotonically increase with θ , reaching a factor of $H_c(80^\circ)/H_c(0^\circ)$ as 1.6–2.0 [70–73,75], indicating that DW pinning process is dominant for the magnetization reversal of the exchange-coupled magnets. An analogous phenomenon which may correlate with the angular dependence of coercivity is that the coercivity of Nd-Fe-B magnet monotonically decreases with the degree of grain alignment [77], which is also explained in simulation by Fujisaki et al. [78] as the result of DW pinning at grain boundaries. Interestingly, for those GB-engineered magnets with a large fraction of Nd-rich nonferromagnetic intergranular phases, the pinning feature of $H_c(\theta)$ becomes weak while nucleation feature tends to emerge. For example, a very slowly increasing $H_c(\theta)$ was observed for the optimally annealed Ga-doped Nd-rich B-lean sintered magnet (Figure 15(a)), and a slowly varying $H_c(\theta)$ with a weak ‘dip’ was observed for the hot-deformed magnet with a heavy infiltration of Nd-Cu alloy [75]. These slowly varying $H_c(\theta)$ deviates from a monotonically and sharply increasing $H_c(\theta)$ observed in the simulated pinning-control reversal, and also largely deviate from that of an ideally exchange-decoupled model which shows Stoner–Wohlfarth-like curve [76], indicating that the mechanism of H_c here should not be simply described as pinning- or nucleation-control. Therefore, from the

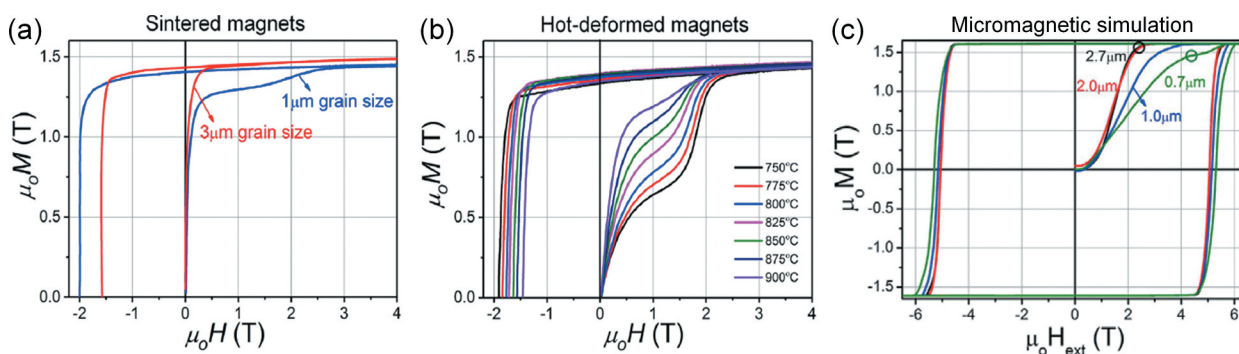


Figure 14. (a) Initial and demagnetization curves of sintered magnet with different grain sizes [66]. (b) Initial and demagnetization curves of hot-deformed magnet with different grain sizes [67]. (c) Simulated initial curves and hysteresis loops of models with different grain sizes [44]. Reproduced from Sepehri-Amin et al. [44,66] and Liu et al. [67] with copyright permissions from Elsevier.

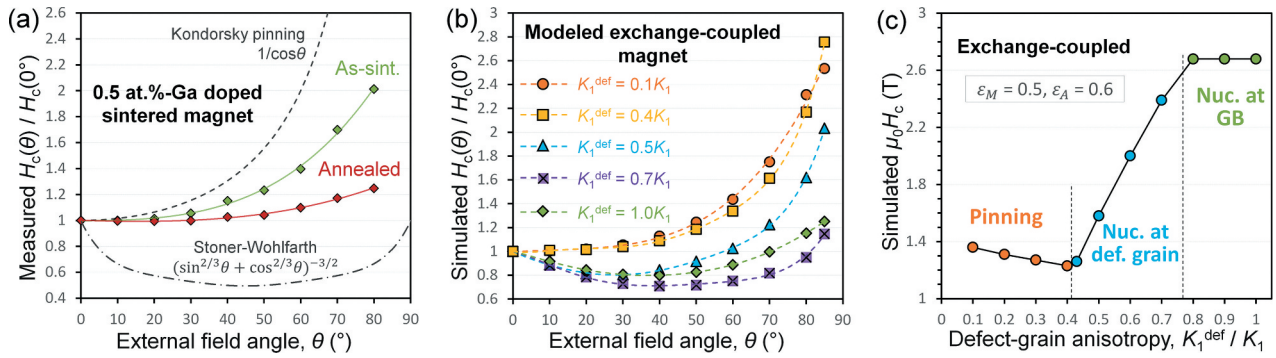


Figure 15. (a) Angular dependence of coercivity of Ga-doped sintered Nd-Fe-B magnet with or without post-sinter annealing. (b) Simulated angular dependence of coercivity of a modeled polycrystalline Nd-Fe-B magnet. (c) The simulated $H_c(0^\circ)$ corresponding to (b), where the reversal mechanism is controlled by the anisotropy energy of the defect grain, K_1^{def} . Reproduced by permission from [76], copyright (2020, Elsevier).

angular dependence of H_c , it is concluded that the H_c mechanism is typical pinning type for the exchange-coupled sintered magnet and hot-deformed magnet. Micromagnetic simulation indicates that the mechanism would change to the nucleation type when grains are perfectly exchange decouples, while such exchange-decoupled magnets have not been demonstrated in the Nd-Fe-B system.

In short, the coercivity of the exchange-coupled Nd-Fe-B magnets can be explained by the DW pinning at the grain boundaries. The absence of the pinning feature in the initial magnetization curve is merely due to the multidomain state of large grains of the standard sintered magnets. When grain size becomes comparable to the domain size ($\sim 1 \mu\text{m}$), the DW pinning by grain boundaries become visible in the initial magnetization curve. When grains are exchange decoupled by the formation of nonferromagnetic intergranular phase, the magnetization mechanism is expected to transfer to the nucleation mechanism, by which higher coercivity will be achieved.

7. How to improve the thermal stability of H_c ?

High-temperature application is always a challenge for Nd-Fe-B magnet due to the severe reduction of H_c at elevated temperature. One long-standing question about the temperature dependence of coercivity is its nonlinear change with concavity downwards with respect to the change of $H_A(T)$ as shown in Figure 16 (a). The discrepancy between $H_c(T)$ and $H_A(T)$ cannot be explained with the well-known equation of coercivity, $H_c = \alpha H_A - N_{\text{eff}} M_s$, which predicts linear correlation between $H_c(T)$ and $H_A(T)$ since microstructure parameter α was assumed to be constant. Recently, Li et al. [79] reproduced the concavity of $H_c(T)$ in the micromagnetic simulations (Figure 16(b)) that considered the temperature dependence of GB magnetization adapted from XMCD measurements [23]. It is

explained that the parameter α is also temperature-dependent since the GB magnetization follows different temperature dependence with respect to that of $\text{Nd}_2\text{Fe}_{14}\text{B}$. Following this argument, the magnet with reduced GB magnetization should exhibit linear change of $H_c(T)$ [79]. In fact, the linear $H_c(T)$ has been reported in several works on eutectic diffusion processed hot-deformed magnet [61–63] without any insight on the underlying mechanism.

Conventionally, the thermal stability of coercivity of Nd-Fe-B magnet is quantitatively described by its temperature coefficient, $\beta_{H_c} = \frac{\Delta H_c}{H_c(RT)\Delta T}$, where a small negative value of β_{H_c} guarantees a small relative change (reduction) of H_c . The typical value of β_{H_c} for Dy-free sintered magnet is $\sim -0.6\% \text{ K}^{-1}$ at 160°C . An important feature about β_{H_c} is that, like coercivity, it is microstructure controlled and thus can be improved via magnet processing. By substituting Kronmüller’s equation in the expression of β_{H_c} [63,80], it is found that improved value of β_{H_c} can be achieved in a microstructure with large value of α or small value of N_{eff} . Grain size reduction is one way to improve the thermal stability of coercivity as demonstrated by Liu et al. [67] which originates from the reduction of N_{eff} in smaller grain-sized magnets. In hot-deformed magnets, N_{eff} can be reduced by decreasing the aspect ratio of the platelet-like grains [81], which lead to a moderate improvement of β_{H_c} [82]. On the other hand, large α value means the diminish of the defects with low anisotropy field such as ferromagnetic grain boundaries or soft-magnetic intergranular phase. Improvement of β_{H_c} via increased α has been demonstrated in GB engineered Nd-Fe-B magnets, e.g. the Ga-doped Nd-rich B-lean sintered magnet after optimized annealing process [76], or the hot-deformed magnets that were diffusion processed with Nd_xM_y ($M = \text{Cu}, \text{Al}, \text{Ga}$ et al.) eutectic alloys [60,61,83–85]. The Nd-Cu eutectic diffusion process applied to a hot-deformed magnet improved β_{H_c} to around $-0.40\% \text{ K}^{-1}$ at 500 K (see

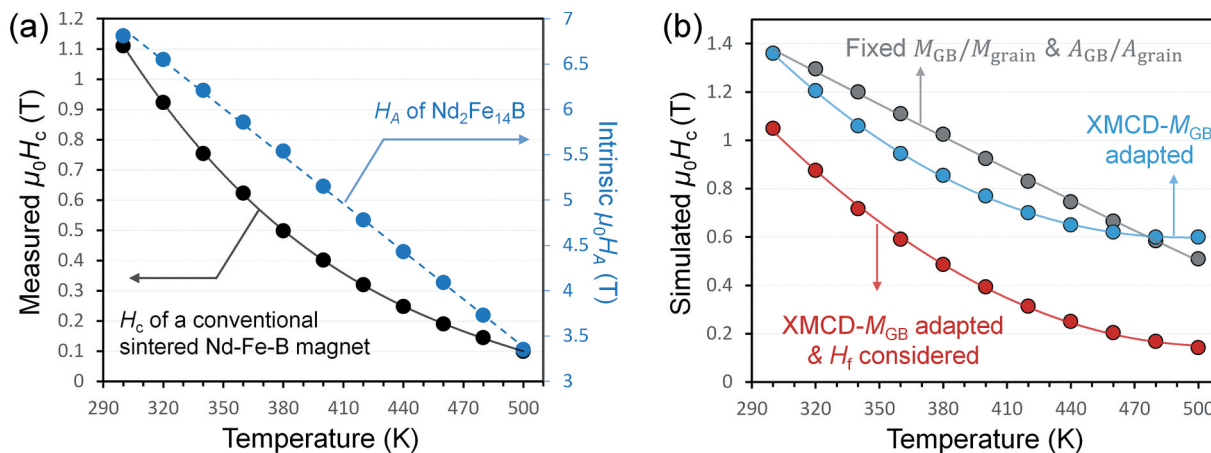


Figure 16. (a) Comparison of $H_A(T)$ and $H_c(T)$ of a conventional Nd-Fe-B sintered magnet. (b) Simulated $H_c(T)$ of a modeled sintered magnet. Reproduced by permission from [79], copyright (2020, Elsevier).

Figure 17(a,b)). Tang et al. [86] demonstrated that the application of the Nd-Cu diffusion process to (Nd_{0.8}Ce_{0.2})-Fe-B hot-deformed magnet also led to a substantial improvement of the thermal stability of H_c , giving rise to the higher H_c at elevated temperature that is superior to that of Nd-Fe-B magnets.

The formation of core-shell structure in HRE eutectic diffusion processed magnet was also found to be effective in improving the thermal stability of coercivity. Benefiting from the good thermal stability of H_A of Tb₂Fe₁₄B phase, Nd₆₀Tb₂₀Cu₂₀ eutectic diffusion processed Nd-Fe-B hot-deformed magnet was found to show substantially improved β_{H_c} of $-0.3\% K^{-1}$ (500 K) as shown in Figure 17(b) [63], much superior to that of Nd₇₀Cu₃₀ eutectic diffusion processed sample. Micromagnetic simulations by Li et al. [63] suggested that the formation of Tb-rich shell improves the thermal stability of coercivity in both exchange-coupled and exchange-decoupled grain models. On the contrary, the thermal stability of Pr₈₀Cu₂₀ diffusion processed magnet was found inferior to that of Nd₈₀Cu₂₀ diffusion processed sample [87], as a result of the poor thermal stability of Pr₂Fe₁₄B H_A .

In short, the thermal stability of coercivity can be improved in the same approach of improving coercivity without using HRE, i.e. reducing the grain size, tuning the grain shape and modifying the GB magnetism, and it can be further improved by introducing (Nd,HRE)₂Fe₁₄B shell in Nd₂Fe₁₄B grains. In particular, modifying GB to nonferromagnetic can suppress the concavity of $H_c(T)$ curve and change the shape closer to $H_A(T)$.

8. Why does Ce-substituted (Nd_{1-x}Ce_x)-Fe-B magnets show improved thermal stability of coercivity?

The ever-increasing demands on the Nd-Fe-B-based permanent magnets has raised concerns on the future supply chain of Nd which is the main rare-earth element used in these magnets. Although Nd is relatively abundant middle rare-earth elements, light rare earth (LRE) elements are always produced as byproducts and its effective usage is expected to reduce the entire cost of industrially useful rare-earth elements. Pathak et al. proposed the possibility of cost-effective

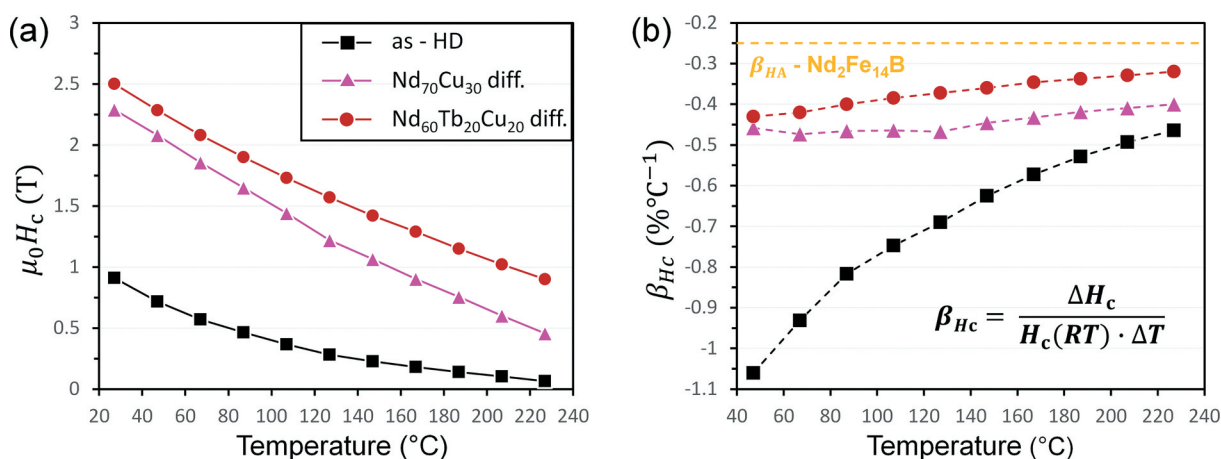


Figure 17. (a) Temperature dependence of coercivity of as-hot-deformed and eutectic diffusion-processed Nd-Fe-B magnets [63]. (b) The temperature coefficient of coercivity for samples in (a). Reproduced by permission from [63], copyright (2018, Elsevier).

permanent magnets by substituting part of Nd with LRE element, Ce, for Nd [88]. Since then, many investigations have been carried out to optimize the permanent magnetic properties of both isotropic and anisotropic $(\text{Nd}_{1-x}\text{LRE}_x)\text{-Fe-B}$ magnets [89–94]. However, the intrinsic magnetic properties of $\text{LRE}_2\text{Fe}_{14}\text{B}$ compounds are inferior to those of $\text{Nd}_2\text{Fe}_{14}\text{B}$, limiting the performance of LRE-substituted permanent magnets; e.g. $\text{Ce}_2\text{Fe}_{14}\text{B}$ compound has $\mu_0 H_A = 2.6\text{ T}$, $\mu_0 M_s = 1.17\text{ T}$ and $T_c = 150^\circ\text{C}$ with respect to $\mu_0 H_A = 7.5\text{ T}$, $\mu_0 M_s = 1.6\text{ T}$ and $T_c = 320^\circ\text{C}$ for $\text{Nd}_2\text{Fe}_{14}\text{B}$ [95]. Recent studies on the intrinsic magnetic properties of single crystalline $(\text{Nd}_{1-x}\text{Ce}_x)_2\text{Fe}_{14}\text{B}$ by Susner et al. [96] have shown that the magnetization ($M_s/\text{f.u.}$) and anisotropy field can be well preserved up to $x = 0.22$. Hence, limited substitution of LRE elements such as Ce for Nd is expected to minimize the degradation of hard magnetic properties of $(\text{Nd}_{1-x}\text{Ce}_x)\text{-Fe-B}$ -based magnets. An early work of Zhu et al. [97] reported a coercivity of 1.2 T and remanence of 1.37 T in $(\text{Nd,Ce})\text{-Fe-B}$ sintered magnet prepared by so-called ‘dual alloy’ method which utilized mixed Nd-Fe-B and $(\text{Nd,Ce})\text{-Fe-B}$ powders for sintering. Fan et al. [98] also showed by limited usage of Ce, i.e. 25% substitution of Nd for Ce, a moderate coercivity of 1.21 T and a remanence of 1.33 T can be achieved in $(\text{Nd,Ce})\text{-Fe-B}$ sintered magnets. However, these moderate magnetic properties are still far to consider $(\text{Nd,Ce})\text{-Fe-B}$ -based permanent magnets as high-performance magnets. In addition to the intrinsic origins for the deterioration of coercivity and remanent magnetization, the formation of undesired phases such as CeFe_2 and the lack of RE-rich intergranular phase were found to be a microstructure origin for the inferior extrinsic magnetic properties in the $(\text{Nd,Ce})\text{-Fe-B}$ magnets [97,99,100].

Recently, TOYOTA motor corporation announced that a LRE-substituted hot-deformed magnet showed superior temperature coefficient of coercivity compared to the conventional sintered magnets [101]. However, its scientific origin has not been reported. To trace the announced result scientifically, Tang et al. [86] demonstrated a $(\text{Nd}_{0.8}\text{Ce}_{0.2})\text{-Fe-B}$ -based hot-deformed magnet exhibits the permanent magnet properties comparable to those for N42H class commercial sintered magnet as shown in Figure 18. The coercivity was further enhanced to 1.83 T by optimizing the microstructure using the Nd-Cu eutectic alloy diffusion process to the $(\text{Nd}_{0.75}\text{Ce}_{0.25})\text{-Fe-B}$ hot-deformed magnets as the result of the formation of (Nd,Ce,Cu) -rich intergranular phase. The formation of Nd-rich 2:14:1 shell covering $(\text{Nd}_{0.75}\text{Ce}_{0.25})_2\text{Fe}_{14}\text{B}$ was another microstructure feature responsible for enhancement of coercivity. Although the Curie temperature of $\text{Ce}_2\text{Fe}_{14}\text{B}$ is much lower than that of $\text{Nd}_2\text{Fe}_{14}\text{B}$, the 20%Ce-substituted anisotropic magnet showed the hard magnetic properties comparable to those of N42H-grade commercial sintered magnet with a similar RE concentration of 15 at.% as shown in Figure 18(a). The Ce-substituted magnet showed a temperature coefficient of coercivity of $-0.59\%/^\circ\text{C}$, which is superior to that of N42H. The origin of the improved temperature coefficient of coercivity of the Ce-substituted hot-deformed magnets was attributed to the low magnetization of the (Nd,Ce) -enriched intergranular phase and the formation of high- H_A Nd-rich shell. These reports clearly show $(\text{Nd,Ce})\text{-Fe-B}$ -based hot-deformed magnets with optimized microstructure can be considered as low-cost high-performance permanent magnets [86].

In short, serious degradation of coercivity and remanence by substituting Nd with Ce in Nd-Fe-B magnet can be avoided by the microstructure

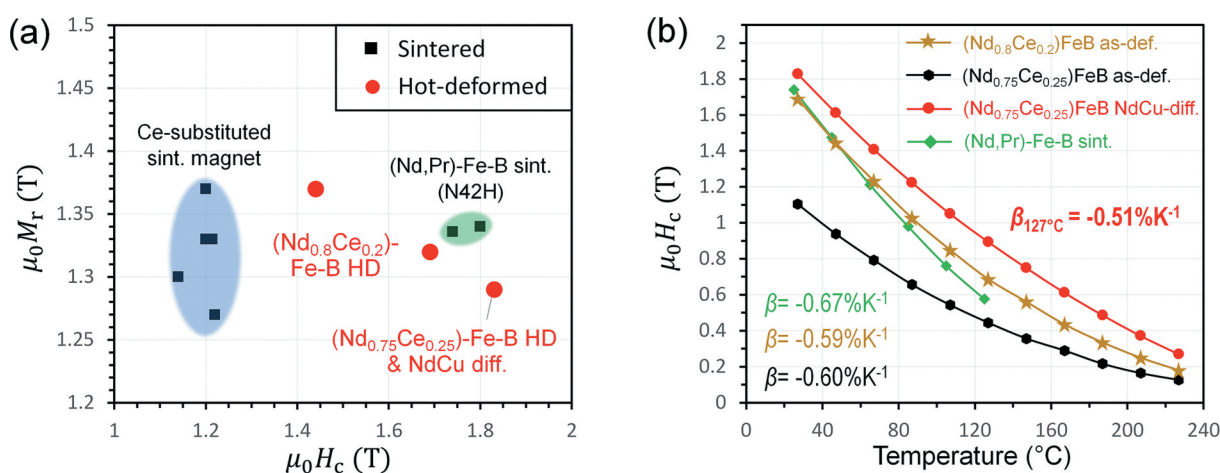


Figure 18. (a) Remanence versus coercivity of Ce-substituted sintered magnets with 18–27 at.% Ce substitution for Nd [97,98,102,103], and of hot-deformed magnets with 20 at.% Ce substitution for Nd. The N42H-grade sintered magnets [104] is plotted for comparison. (b) Temperature dependence of coercivity of $(\text{Nd,Pr})\text{-Fe-B}$ sintered magnet with RE concentration of 15 at.%, hot-deformed $(\text{Nd}_{0.8}\text{Ce}_{0.2})\text{-Fe-B}$ magnet with RE concentration of 14.5 at.%, hot-deformed $(\text{Nd}_{0.75}\text{Ce}_{0.25})\text{-Fe-B}$ magnet, and Nd-Cu diffusion processed $(\text{Nd}_{0.75}\text{Ce}_{0.25})\text{-Fe-B}$ hot-deformed magnet. Reproduced by permission from [86], copyright (2020, Elsevier).

optimization as long as the Ce concentration ratio, Ce/RE, is controlled smaller than 30%. The origin of the improved temperature coefficient of coercivity is the formation of (Nd,Ce)-rich intergranular phase and Nd-rich shell.

9. What is the Nd-Fe-B magnet with ultimate performance?

The ultimate performance of coercivity and its thermal stability is expected in a magnet with maximized anisotropy factor α as well as minimized demagnetization factor N_{eff} to approach the limit of intrinsic H_A . Factor α can be maximized by the formation of nonferromagnetic intergranular phase isolating every 2:14:1 grain, resulting in a pure nucleation-control magnetization reversal in the magnet. Reducing grain size is the conventional and practical way to minimize N_{eff} . However, this approach failed in the magnet with submicron grain size which was produced by hydrogenation–disproportionation–desorption–recombination (HDDR) and press-less sintering process (PLP) since the thin intergranular phase is ferromagnetic [105]. This result suggests the importance of the formation of nonferromagnetic GB phase fully isolating $\text{Nd}_2\text{Fe}_{14}\text{B}$ grains. The hot-deformed magnets which consist of submicron-sized grains show $\mu_0 H_c$ values in the range of 1.0–2.0 T that are comparable with that of sintered magnets with a grain size generally much larger than 1 μm . Although the engineering of the intergranular phase via eutectic diffusion process in the hot-deformed magnets results in a substantial enhancement of coercivity, further enhancement of coercivity is expected if the side GB phase can also become paramagnetic. Note that the current experimental knowledge has no answer on how to fully exchange decoupled $\text{Nd}_2\text{Fe}_{14}\text{B}$ grains in the anisotropic ultra-fine grain-sized Nd-Fe-B magnets.

On the other hand, the volume fraction of intergranular phase increases with reducing grain size, which will lead to a drop of remanence if all the grain boundaries are nonferromagnetic. As a simple demonstration, the volume fraction of intergranular phase in a stack of cubit blocks is given by $f_{\text{GB}} = \frac{(L/D)^3 \cdot 3D^2 \cdot t}{L^3} = \frac{3t}{D}$, where L is the total size, D is the block size and t is the thickness of the intergranular phase. For a GB thickness of $t = 3$ nm and a requirement of limited volume fraction of GB, e.g. $f_{\text{GB}} \leq 10\%$ ($\frac{M_{\text{magnet}}}{M_{2:14:1}} \geq 90\%$), one has $D \geq 90\text{nm}$. This simple calculation indicates that the optimized grain size of a Nd-Fe-B magnet is in the order of 100 nm, and further reduction of grain size is not suggested since the volume fraction of the intergranular phase becomes too large and the degradation of remanence is unavoidable.

Based on the above discussion, the ultimate performance of extrinsic property is expected in a magnet with grain size around several hundred nanometers, equiaxed shape, uniformly separated by nonferromagnetic intergranular phase (i.e. exchange isolated). As a reference, micromagnetic simulation consisting of exchange-decoupled equiaxed grains with a size of 100 nm predicted a coercivity of 3.5 T ($\sim H_A/2$) [79]. The formation of high- H_A shell enveloping the exchange-decoupled $\text{Nd}_2\text{Fe}_{14}\text{B}$ grains can further improve H_c and β_{H_c} to overcome the limit of intrinsic H_A of the $\text{Nd}_2\text{Fe}_{14}\text{B}$ phase. Since its mechanism is to force a relocation of nucleation site from grain surface to the core/shell interface where the demagnetizing field is smaller [63], H_c and β_{H_c} will increase gradually with the increase of shell thickness when grain size is fixed. The enrichment of Dy or Tb at the thin shell region is needed which shows intrinsic β_{H_A} comparable or even better than $\text{Nd}_2\text{Fe}_{14}\text{B}$.

The recent advances on the multi-scale microstructure characterizations have broadened our understanding on the coercivity mechanism of Nd-Fe-B-based magnets leading to a substantial improvement on coercivity and its thermal stability in the last decade. However, still there is a gap between the experimentally achieved coercivity ($\square H_A/3$) and the simulation predicted coercivity in an optimal microstructure ($\sim H_A/2$). It is expected to fill the gap by further reduction of the grain size and magnetic isolation of $\text{Nd}_2\text{Fe}_{14}\text{B}$ grains with thin nonferromagnetic intergranular phase, which has not been realized yet. Materials informatics and active learning [106–109], which has not been used seriously in the permanent magnet community, can pave a way for raising novel ideas on how to further optimize the microstructure of ultra-fine grain sized anisotropic Nd-Fe-B magnets. Hence, revisiting the accumulated knowledge on the phase diagram, processing, and microstructure of Nd-Fe-B-based magnets and employing materials informatics can be tools to realize Nd-Fe-B-based permanent magnets with ultimate performance without reliance on heavy rare-earth elements.

Disclosure statement

No potential conflict of interest was reported by the author(s).

Funding

This work was in-part supported by JST, Collaborative Research Based on Industrial Demand, Grant Number [PMJSK1618], and Elements Strategy Initiative Center for Magnetic Materials (ESICMM), Grant Number [JPMXP0112101004], through the Ministry of Education, Culture, Sports, Science and Technology (MEXT). We thank Dr. Masato Sagawa and Dr. Satoshi Hirosawa for valuable discussions throughout study on Nd-Fe-B permanent magnet materials.

ORCID

Jiangnan Li  <http://orcid.org/0000-0003-1306-3062>
 Hossein Sepehri-Amin  <http://orcid.org/0000-0002-7856-7897>
 Taisuke Sasaki  <http://orcid.org/0000-0002-5952-7638>
 Tadakatsu Ohkubo  <http://orcid.org/0000-0003-3548-1951>
 Kazuhiro Hono  <http://orcid.org/0000-0001-7367-0193>

References

- [1] Sagawa M, Fujimura S, Togawa N, et al. New material for permanent magnets on a base of Nd and Fe. *J Appl Phys.* 1984;55:2083–2087.
- [2] Croat JJ, Herbst JF, Lee RW, et al. Pr-Fe and Nd-Fe-based materials: a new class of high-performance permanent magnets. *J Appl Phys.* 1984;55:2078–2082.
- [3] Yang Y, Walton A, Sheridan R, et al. REE recovery from end-of-life NdFeB permanent magnet scrap: a critical review. *J Sustain Metall.* 2017;3:122–149.
- [4] Sagawa M, Fujimura S, Yamamoto H, et al. Permanent magnet materials based on the rare earth-iron-boron tetragonal compounds. *IEEE Trans Magn.* 1984;20:1584–1589.
- [5] Hirosawa S, Matsuura Y, Yamamoto H, et al. Magnetization and magnetic anisotropy of $R_2Fe_{14}B$ measured on single crystals. *J Appl Phys.* 1986;59:873–879.
- [6] Hono K, Sepehri-Amin H. Strategy for high-coercivity Nd-Fe-B magnets. *Scr Mater.* 2012;67:530–535.
- [7] Hono K, Sepehri-Amin H. Prospect for HRE-free high coercivity Nd-Fe-B permanent magnets. *Scr Mater.* 2018;151:6–13.
- [8] Mishra RK, Chen JK, Thomas G. Effect of annealing on the microstructure of sintered Nd-Fe-B magnets. *J Appl Phys.* 1986;59:2244–2246.
- [9] Fidler J, Bernardi J. Transmission electron microscope characterization of cast and hot-worked R-Fe-B:Cu(R =Nd,Pr) permanent magnets. *J Appl Phys.* 1991;70:6456–6458.
- [10] Engelmann HJ, Kim AS, Thomas G. Microstructure and magnetic effects of small Cu additions to (Nd,Dy) FeB magnets. *Scr Mater.* 1997;36:55–62.
- [11] Bernardi J, Fidler J. Preparation and transmission electron microscope investigation of sintered $Nd_{15.4}Fe_{75.7}B_{6.7}Cu_{1.3}Nb_{0.9}$ magnets. *J Appl Phys.* 1994;76:6241–6243.
- [12] Vial F, Joly F, Nevalainen E, et al. Improvement of coercivity of sintered NdFeB permanent magnets by heat treatment. *J Magn Magn Mater.* 2002; 242–245:1329–1334.
- [13] Velicescu M, Fernengel W, Rodewald W, et al. High-energy sintered Nd-Dy-Fe-B magnets with Co and Cu additions. *J Magn Magn Mater.* 1996;157–158:47–48.
- [14] Gabay AM, Zhang Y, Hadjipanayis GC. Effect of very small additions on the coercivity of Dy-free Nd-Fe-(Co)-B-sintered magnets. *J Magn Magn Mater.* 2002;238:226–232.
- [15] Pandian S, Chandrasekaran V, Markandeyulu G, et al. Effect of Al, Cu, Ga, and Nb additions on the magnetic properties and microstructural features of sintered NdFeB. *J Appl Phys.* 2002;92:6082–6086.
- [16] Ahmad I, Davies HA, Buckley RA. Ultra high coercivity Nd-Fe-B permanent magnet alloy with small addition of Ga. *Mater Lett.* 1994;20:139–142.
- [17] Yan A, Song X, Chen Z, et al. Characterization of microstructure and coercivity of Nd-Fe-B magnets with Ti and Al or Cu addition. *J Magn Magn Mater.* 1998;185:369–374.
- [18] Li WF, Ohkubo T, Akiya T, et al. The role of Cu addition in the coercivity enhancement of sintered Nd-Fe-B permanent magnets. *J Mater Res.* 2009;24:413–420.
- [19] Li WF, Ohkubo T, Hono K. Effect of post-sinter annealing on the coercivity and microstructure of Nd-Fe-B permanent magnets. *Acta Mater.* 2009; 57:1337–1346.
- [20] Fidler J, Schrefl T. Overview of Nd-Fe-B magnets and coercivity. *J Appl Phys.* 1996;79:5029.
- [21] Sepehri-Amin H, Ohkubo T, Shima T, et al. Grain boundary and interface chemistry of an Nd-Fe-B-based sintered magnet. *Acta Mater.* 2012; 60:819–830.
- [22] Fidler J, Schrefl T, Sasaki S, et al. The role of intergranular regions in sintered Nd-Fe-B magnets with $(BH)_{max} < 420 \text{ kJ/m}^3$ (52.5 MGOe). Proceedings of XI Int. Symposium on Magnetic Anisotropy and Coercivity in Rare Earth Transition Metal Alloys, Sendai, Japan; 2000.
- [23] Nakamura T, Yasui A, Kotani Y, et al. Direct observation of ferromagnetism in grain boundary phase of Nd-Fe-B sintered magnet using soft x-ray magnetic circular dichroism. *Appl Phys Lett.* 2014;105:202404.
- [24] Kohashi T, Motai K, Nishiuchi T, et al. Magnetism in grain-boundary phase of a NdFeB sintered magnet studied by spin-polarized scanning electron microscopy. *Appl Phys Lett.* 2014;104:232408.
- [25] Murakami Y, Tanigaki T, Sasaki TT, et al. Magnetism of ultrathin intergranular boundary regions in Nd-Fe-B permanent magnets. *Acta Mater.* 2014;71: 370–379.
- [26] Schrefl T, Fidler J, Kronmüller H. Remanence and coercivity in isotropic nanocrystalline permanent magnets. *Phys Rev B.* 1994;49:6100–6110.
- [27] Fujisaki J, Furuya A, Uehara Y, et al. Micromagnetic simulation of the orientation dependence of grain boundary properties on the coercivity of Nd-Fe-B sintered magnets. *AIP Adv.* 2016;6:056028.
- [28] Sasaki TT, Ohkubo T, Hono K. Structure and chemical compositions of the grain boundary phase in Nd-Fe-B sintered magnets. *Acta Mater.* 2016;115:269–277.
- [29] Sakuma A, Suzuki T, Furuuchi T, et al. Magnetism of Nd-Fe films as a model of grain boundary phase in Nd-Fe-B permanent magnets. *Appl Phys Express.* 2016;9:013002.
- [30] Fidler J, Groiss C, Tokunaga M. The influence of Ga-substitution on the coercivity of Nd-(Fe,Co)-B sintered permanent magnets. *IEEE Trans Magn.* 1990;26:1948–1950.
- [31] Bernardi J, Fidler J, Seeger M, et al. Preparation and TEM-study of sintered $Nd_{18}Fe_{74}B_6Ga_1Nb_1$ magnets. *IEEE Trans Magn.* 1993;29:2773–2775.
- [32] Tokunaga M, Kogure H, Endoh M, et al. Improvement of thermal stability of Nd-Dy-Fe-Co-B sintered magnets by additions of Al, Nd and Ga. *IEEE Trans Magn.* 1987;23:2287–2289.
- [33] Tsutai A, Sakai I, Mizoguchi T, et al. Effect of Ga addition to NdFeCoB on their magnetic properties. *Appl Phys Lett.* 1987;51:1043–1045.
- [34] Nakajima K, Yamazaki T. Japan Patent. 2015; 5767788.
- [35] Sasaki TT, Ohkubo T, Takada Y, et al. Formation of non-ferromagnetic grain boundary phase in a Ga-

- doped Nd-rich Nd-Fe-B sintered magnet. *Scr Mater.* **2016**;113:218–221.
- [36] Niitsu K, Sato A, Sasaki TT, et al. Magnetization measurements for grain boundary phases in Ga-doped Nd-Fe-B sintered magnet. *J Alloys Compd.* **2018**;752:220–230.
- [37] Soderžnik M, Sepehri-Amin H, Sasaki TT, et al. Magnetization reversal of exchange-coupled and exchange-decoupled Nd-Fe-B magnets observed by magneto-optical Kerr effect microscopy. *Acta Mater.* **2017**;135:68–76.
- [38] Ramesh R, Srikrishna K. Magnetization reversal in nucleation controlled magnets. I. Theory. *J Appl Phys.* **1988**;64:6406–6415.
- [39] Nothnagel P, Müller KH, Eckert D, et al. The influence of particle size on the coercivity of sintered NdFeB magnets. *J Magn Magn Mater.* **1991**;101:379–381.
- [40] Uestuener K, Katter M, Rodewald W. Dependence of the mean grain size and coercivity of sintered Nd-Fe-B magnets on the initial powder particle size. *IEEE Trans Magn.* **2006**;42:2897–2899.
- [41] Li WF, Ohkubo T, Hono K, et al. The origin of coercivity decrease in fine grained Nd-Fe-B sintered magnets. *J Magn Magn Mater.* **2009**;321:1100–1105.
- [42] Une M, Sagawa Y. Enhancement of coercivity of the Nd-Fe-B sintered magnets by decreasing the grain size. *Proceeding of the 21st Workshop Rare-earth Permanent Magnets and Their Applications*; Bled, Slovenia; **2010**.
- [43] Schrefl T, Schmidts HF, Fidler J, et al. Nucleation fields and grain boundaries in hard magnetic materials. *IEEE Trans Magn.* **1993**;29:2878–2880.
- [44] Sepehri-Amin H, Ohkubo T, Gruber M, et al. Micromagnetic simulations on the grain size dependence of coercivity in anisotropic Nd-Fe-B sintered magnets. *Scr Mater.* **2014**;89:29–32.
- [45] Kronmüller H, Durst KD, Sagawa M. Analysis of the magnetic hardening mechanism in RE-FeB permanent magnets. *J Magn Magn Mater.* **1988**;74:291–302.
- [46] Billington D, Toyoki K, Okazaki H, et al. Unmasking the interior magnetic domain structure and evolution in Nd-Fe-B sintered magnets through high-field magnetic imaging of the fractured surface. *Phys Rev Mater.* **2018**;2:104413.
- [47] Park KT, Hiraga K, Sagawa M. Effect of metal coating and consecutive heat treatment on coercivity of thin Nd-Fe-B sintered magnets. *Proceeding of the 16th Workshop Rare-earth Permanent Magnets and Their Applications*; Sendai, Japan; **2000**.
- [48] Nakamura H, Hirota K, Shimao M, et al. Magnetic properties of extremely small Nd-Fe-B sintered magnets. *IEEE Trans Magn.* **2005**;41:3844–3846.
- [49] Hirota K, Nakamura H, Minowa T, et al. Coercivity enhancement by the grain boundary diffusion process to Nd-Fe-B sintered magnets. *IEEE Trans Magn.* **2006**;42:2909–2911.
- [50] Watanabe N, Itakura M, Kuwano N, et al. Microstructure analysis of sintered Nd-Fe-B magnets improved by Tb-vapor sorption. *Mater Trans.* **2007**;48:915–918.
- [51] Suzuki H, Satsu Y, Komuro M. Magnetic properties of a Nd-Fe-B sintered magnet with Dy segregation. *J Appl Phys.* **2009**;105:07A734.
- [52] Li D, Suzuki S, Kawasaki T, et al. Grain interface modification and magnetic properties of Nd-Fe-B sintered magnets. *Jpn J Appl Phys.* **2008**;47:7876–7878.
- [53] Samardžija Z, McGuinness P, Soderžnik M, et al. Microstructural and compositional characterization of terbium-doped Nd-Fe-B sintered magnets. *Mater Charact.* **2012**;67:27–33.
- [54] Sepehri-Amin H, Ohkubo T, Hono K. The mechanism of coercivity enhancement by the grain boundary diffusion process of Nd-Fe-B sintered magnets. *Acta Mater.* **2013**;61:1982–1990.
- [55] Kim TH, Sasaki TT, Ohkubo T, et al. Microstructure and coercivity of grain boundary diffusion processed Dy-free and Dy-containing Nd-Fe-B sintered magnets. *Acta Mater.* **2019**;172:139–149.
- [56] Seelam UMR, Ohkubo T, Abe T, et al. Faceted shell structure in grain boundary diffusion-processed sintered Nd-Fe-B magnets. *J Alloys Compd.* **2014**;617:884–892.
- [57] Kim TH, Sasaki TT, Koyama T, et al. Formation mechanism of Tb-rich shell in grain boundary diffusion processed Nd-Fe-B sintered magnets. *Scr Mater.* **2020**;178:433–437.
- [58] Sepehri-Amin H, Liu J, Ohkubo T, et al. Enhancement of coercivity of hot-deformed Nd-Fe-B anisotropic magnet by low-temperature grain boundary diffusion of Nd₆₀Dy₂₀Cu₂₀ eutectic alloy. *Scr Mater.* **2013**;69:647–650.
- [59] Sepehri-Amin H, Ohkubo T, Nishiuchi T, et al. Coercivity enhancement of hydrogenation-disproportionation-desorption-recombination processed Nd-Fe-B powders by the diffusion of Nd-Cu eutectic alloys. *Scr Mater.* **2010**;63:1124–1127.
- [60] Sepehri-Amin H, Ohkubo T, Nagashima S, et al. High-coercivity ultrafine-grained anisotropic Nd-Fe-B magnets processed by hot deformation and the Nd-Cu grain boundary diffusion process. *Acta Mater.* **2013**;61:6622–6634.
- [61] Liu L, Sepehri-Amin H, Ohkubo T, et al. Coercivity enhancement of hot-deformed Nd-Fe-B magnets by the eutectic grain boundary diffusion process. *J Alloys Compd.* **2016**;666:432–439.
- [62] Liu L, Sepehri-Amin H, Ohkubo T, et al. Coercivity enhancement of hot-deformed Nd-Fe-B magnets by the eutectic grain boundary diffusion process using Nd₆₂Dy₂₀Al₁₈ alloy. *Scr Mater.* **2017**;129:44–47.
- [63] Li J, Liu L, Sepehri-Amin H, et al. Coercivity and its thermal stability of Nd-Fe-B hot-deformed magnets enhanced by the eutectic grain boundary diffusion process. *Acta Mater.* **2018**;161:171–181.
- [64] Handstein A, Schneider J, Stephan D, et al. Reversal of magnetization in Nd-Fe-B magnets. *Mater Lett.* **1985**;3:200–205.
- [65] Hadjipanayis GC, Kim A. Domain wall pinning versus nucleation of reversed domains in R-Fe-B magnets. *J Appl Phys.* **1988**;63:3310–3315.
- [66] Sepehri-Amin H, Une Y, Ohkubo T, et al. Microstructure of fine-grained Nd-Fe-B sintered magnets with high coercivity. *Scr Mater.* **2011**;65:396–399.
- [67] Liu J, Sepehri-Amin H, Ohkubo T, et al. Grain size dependence of coercivity of hot-deformed Nd-Fe-B anisotropic magnets. *Acta Mater.* **2015**;82:336–343.
- [68] Kittel C. Physical theory of ferromagnetic domains. *Rev Mod Phys.* **1949**;21:541–583.
- [69] Kronmüller H, Durst KD, Martinek G. Angular dependence of the coercive field in sintered Fe₇₇Nd₁₅B₈ magnets. *J Magn Magn Mater.* **1987**;69:149–157.

- [70] Givord D, Tenaud P, Viadieu T. Angular dependence of coercivity in sintered magnets. *J Magn Magn Mater.* **1988**;72:247–252.
- [71] Givord D, Lu Q, Rossignol MF, et al. Experimental approach to coercivity analysis in hard magnetic materials. *J Magn Magn Mater.* **1990**;83:183–188.
- [72] Martinek G, Kronmüller H. Influence of grain orientation of the coercive field in Fe-Nd-B permanent magnets. *J Magn Magn Mater.* **1990**;86:177–183.
- [73] Cebollada F, Rossignol MF, Givord D, et al. Angular dependence of coercivity in Nd-Fe-B sintered magnets: proof that coherent rotation is not involved. *Phys Rev B.* **1995**;52:13511–13518.
- [74] Stoner EC, Wohlfarth EP. A mechanism of magnetic hysteresis in heterogeneous alloys. *Phil Trans R Soc Lond A.* **1948**;240:599–642.
- [75] Bance S, Oezelt H, Schrefl T, et al. Influence of defect thickness on the angular dependence of coercivity in rare-earth permanent magnets. *Appl Phys Lett.* **2014**;104:182408.
- [76] Li J, Tang X, Sepehri-Amin H, et al. Angular dependence and thermal stability of coercivity of Nd-rich Ga-doped Nd-Fe-B sintered magnet. *Acta Mater.* **2020**;187:66–72.
- [77] Matsuura Y, Hoshijima J, Ishii R. Relation between $\text{Nd}_2\text{Fe}_{14}\text{B}$ grain alignment and coercive force decrease ratio in NdFeB sintered magnets. *J Magn Magn Mater.* **2013**;336:88–92.
- [78] Fujisaki J, Furuya A, Uehara Y, et al. Micromagnetic simulations of magnetization reversal in misaligned multigrain magnets with various grain boundary properties using large-scale parallel computing. *IEEE Trans Magn.* **2014**;50:7100704.
- [79] Li J, Tang X, Sepehri-Amin H, et al. On the temperature-dependent coercivities of anisotropic Nd-Fe-B magnet. *Acta Mater.* **2020**;199:288–296.
- [80] Li R, Zhang HR, Liu Y, et al. Temperature stability of coercivity in mischmetal-Fe-Co-B melt-spun ribbons. *Mater Res Express.* **2018**;5:056101.
- [81] Thielsch J, Suess D, Schultz L, et al. Dependence of coercivity on length ratios in sub-micron $\text{Nd}_2\text{Fe}_{14}\text{B}$ particles with rectangular prism shape. *J Appl Phys.* **2013**;114:223909.
- [82] Tang X, Li J, Miyazaki Y, et al. Relationship between the thermal stability of coercivity and the aspect ratio of grains in Nd-Fe-B magnets: experimental and numerical approaches. *Acta Mater.* **2020**;183:408–417.
- [83] Akiya T, Liu J, Sepehri-Amin H, et al. High-coercivity hot-deformed Nd-Fe-B permanent magnets processed by Nd-Cu eutectic diffusion under expansion constraint. *Scr Mater.* **2014**;81:48–51.
- [84] Liu L, Sepehri-Amin H, Sasaki TT, et al. Coercivity enhancement of Nd-Fe-B hot-deformed magnets by the eutectic grain boundary diffusion process using Nd-Ga-Cu and Nd-Fe-Ga-Cu alloys. *AIP Adv.* **2018**;8:056205.
- [85] Xia X, Liu M, Zhang T, et al. Improvement of thermal stability in hot-deformed Nd-Fe-B magnets by grain refinement. *Scr Mater.* **2020**;178:129–133.
- [86] Tang X, Song SY, Li J, et al. Thermally-stable high coercivity Ce-substituted hot-deformed magnets with 20% Nd reduction. *Acta Mater.* **2020**;190:8–15.
- [87] Sepehri-Amin H, Liu L, Ohkubo T, et al. Microstructure and temperature dependent of coercivity of hot-deformed Nd-Fe-B magnets diffusion processed with Pr-Cu alloy. *Acta Mater.* **2015**;99:297–306.
- [88] Pathak AK, Khan M, Gschneidner KA Jr, et al. Cerium: an unlikely replacement of dysprosium in high performance Nd-Fe-B permanent magnets. *Adv Mater.* **2015**;27:2663–2667.
- [89] Zhang M, Li Z, Shen B, et al. Permanent magnetic properties of rapidly quenched $(\text{La,Ce})_2\text{Fe}_{14}\text{B}$ nanomaterials based on LaCe mischmetal. *J Alloys Compd.* **2015**;651:144–148.
- [90] Pathak AK, Khan M, Gschneidner KA Jr, et al. Magnetic properties of bulk, and rapidly solidified nanostructured $(\text{Nd}_{1-x}\text{Ce}_x)_2\text{Fe}_{14-y}\text{Co}_y\text{B}$ ribbons. *Acta Mater.* **2016**;103:211–216.
- [91] Peng B, Ma T, Zhang Y, et al. Improved thermal stability of Nd-Ce-Fe-B sintered magnets by Y substitution. *Scr Mater.* **2017**;131:11–14.
- [92] Fan X, Chen K, Guo S, et al. Core-shell Y-substituted Nd-Ce-Fe-B sintered magnets with enhanced coercivity and good thermal stability. *Appl Phys Lett.* **2017**;110:172405.
- [93] Skokov KP, Gutfleisch O. Heavy rare earth free, free rare earth and rare earth free magnets – vision and reality. *Scr Mater.* **2018**;154:289–294.
- [94] Tang X, Sepehri-Amin H, Matsumoto M, et al. Role of Co on the magnetic properties of Ce-substituted Nd-Fe-B hot-deformed magnets. *Acta Mater.* **2019**;175:1–10.
- [95] Herbst JF. $\text{R}_2\text{Fe}_{14}\text{B}$ materials: intrinsic properties and technological aspects. *Rev Mod Phys.* **1991**;63:819–898.
- [96] Susner MA, Conner BS, Saparov BI, et al. Flux growth and characterization of Ce-substituted $\text{Nd}_2\text{Fe}_{14}\text{B}$ single crystals. *J Magn Magn Mater.* **2017**;434:1–9.
- [97] Zhu M, Li W, Wang J, et al. Influence of Ce content on the rectangularity of demagnetization curves and magnetic properties of Re-Fe-B magnets sintered by double main phase alloy method. *IEEE Trans Magn.* **2014**;50:1000104.
- [98] Fan X, Guo S, Chen K, et al. Tuning Ce distribution for high performance Nd-Ce-Fe-B sintered magnets. *J Magn Magn Mater.* **2016**;419:394–399.
- [99] Fan X, Ding G, Chen K, et al. Whole process metallurgical behavior of the high-abundance rare-earth elements LRE (La, Ce and Y) and the magnetic performance of $\text{Nd}_{0.75}\text{LRE}_{0.25}\text{-Fe-B}$ sintered magnets. *Acta Mater.* **2018**;154:343–354.
- [100] Tang X, Sepehri-Amin H, Ohkubo T, et al. Coercivity enhancement of hot-deformed Ce-Fe-B magnets by grain boundary infiltration of Nd-Cu eutectic alloy. *Acta Mater.* **2018**;144:884–895.
- [101] Available from: <https://global.toyota/en/newsroom/corporate/21139684.html>
- [102] Zhu M, Han R, Li W, et al. An enhanced coercivity for $(\text{CeNdPr})\text{-Fe-B}$ sintered magnet prepared by structure design. *IEEE Trans Magn.* **2015**;51:2104604.
- [103] Zhang YJ, Ma T, Jin J, et al. Effects of REFe_2 on microstructure and magnetic properties of Nd-Ce-Fe-B sintered magnets. *Acta Mater.* **2017**;128:22–30.
- [104] Ding G, Guo S, Chen L, et al. Effects of the grain size on domain structure and thermal stability of sintered Nd-Fe-B magnets. *J Alloys Compd.* **2018**;735:1176–1180.
- [105] Xu XD, Sasaki TT, Une Y, et al. Origin of the coercivity difference in Nd-Fe-B sintered magnets processed from hydrogenation-disproportionation-desorption-recombination powder and jet-milled powder. *Acta Mater.* **2018**;151:293–300.

- [106] Fischer CC, Tibbetts KJ, Morgan D, et al. Predicting crystal structure by merging data mining with quantum mechanics. *Nat Mater.* 2006;5:641–646.
- [107] Curtarolo S, Hart GLW, Nardelli MB, et al. The high-throughput highway to computational materials design. *Nat Mater.* 2013;12:191–201.
- [108] Ramprasad R, Batra R, Pilia G, et al. Machine learning in materials informatics: recent applications and prospects. *Npj Comput Mater.* 2017;3:54.
- [109] Yuan R, Liu Z, Balachandran PV, et al. Accelerated discovery of large electrostrains in BaTiO₃-based piezoelectrics using active learning. *Adv Mater.* 2018;30:1702884.